

THE ROLE OF THE OCEANS IN THE GLOBAL CARBON CYCLE: AN OVERVIEW

IRINA MARINOV & JORGE L. SARMIENTO

*Program in Atmospheric and Oceanic Sciences
Princeton University, Sayre Hall, Forrestal Campus
Princeton, New Jersey, USA*

imarinov@princeton.edu, jls@splash.princeton.edu

INTRODUCTION

Typical gases such as oxygen tend to be distributed mostly in the atmosphere (99.4%) and less so in the ocean (0.6%). Carbon dioxide is vastly different from such gases, with 98.5% of the pre-industrial CO₂ in the ocean and only 1.5% in the atmosphere. The reason that CO₂ is found preferentially in the ocean is because of its high solubility (thirty times that of oxygen) and because of the hydrolysis reaction it undergoes to form carbonate and bicarbonate ions. The oceanic carbon inventory of total dissolved inorganic carbon (*DIC*) is also influenced by a combination of biologically mediated processes (the biological pump) and physical and chemical processes (the solubility pump). Both the biological and solubility pumps contribute to a higher concentration of *DIC* in the deep ocean, which reduces atmospheric CO₂ relative to what it would be otherwise.

The fact that the largest part of the total carbon inventory is in the ocean suggests that the ocean exerts a dominant control on atmospheric CO₂. Section 1 introduces the carbon pumps and their role in modulating $p\text{CO}_{2\text{ atm}}$ on the glacial-interglacial time scale.

Human activities such as fossil fuel burning, production of cement, and land use change (e.g., tropical deforestation, land conversion for crops) have led to an increase in emissions of carbon dioxide, three quarters of which is due to fossil fuel burning. As a consequence, the partial pressure of carbon dioxide in the atmosphere has increased from 280 ± 10 ppm before the industrial revolution to 373 ppm in 2002, the highest CO₂ level recorded in the past 20 million years. This spectacular increase is similar to the change that occurred in going from glacial to interglacial periods. However, the present increase has happened within less than 200 years, while glacial-interglacial variations occurred on a time scale of thousands of years.

Most of the increase in radiative trapping since preindustrial times has been attributed to anthropogenic CO₂, with a smaller amount due to methane, nitrous oxide, chlorofluorocarbons, and other anthropogenic gases and aerosols. Since only the anthropogenic CO₂ which stays in the atmosphere adds to the greenhouse effect, it is critical that we quantify the amount of CO₂ taken up by ocean and land. Section 2 discusses the mechanisms behind the uptake of anthropogenic CO₂ by the oceans and illustrates them with results from ocean general circulation models (GCMs) and observations.

Anthropogenically induced increases in carbon dioxide and other atmospheric gases result in an increase in direct trapping of long wave radiation emitted from Earth's surface and have most likely led to climate change and global warming (IPCC Report, 2001). The resulting changes in the ocean physics and biology will modify the biological and solubility pumps, which in turn will affect the oceanic carbon uptake. The complex feedback mechanisms between climate change and ocean carbon uptake are discussed in Section 3.

1. BASIC MECHANISMS AT WORK: THE PRE-ANTHROPOGENIC CARBON CYCLE

CO₂ not only dissolves in water but also reacts with it to form bicarbonate (HCO₃⁻) and carbonate (CO₃²⁻) ions. The total dissolved inorganic carbon (*DIC*) is thus

$$DIC = [CO_2] + [HCO_3^-] + [CO_3^{2-}], \quad (1)$$

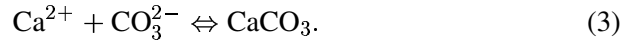
where the fractional contributions of the three species for average surface ocean water are 0.5%, 88.9% and 10.9%, respectively. Total alkalinity (*ALK*) can be defined from a statement of charge balance of the ocean and is well approximated by:

$$ALK \approx [HCO_3^-] + 2 \cdot [CO_3^{2-}] + [B(OH)_4^-] + [OH^-] - [H^+] + others, \quad (2)$$

where $[B(OH)_4^-]$ is the concentration of the borate ion and the fractional contributions of the first three species are 76.8%, 18.8%, and 4.2%, respectively. Observations show that *DIC* varies in the ocean from a surface value of about 1970 umol/kg to deep values of 2280 umol/kg, while *ALK* increases from about 2280 umol/kg at the surface to 2350 umol/kg at depth. What are the processes that maintain these gradients against the homogenizing tendencies of oceanic transport and mixing? What determines the complex features of pre-anthropogenic air-sea CO₂ fluxes? The mechanisms responsible for all of the above are the biological and solubility pumps.

Dissolved inorganic chemicals such as *DIC* and phosphate (PO₄) are consumed by photosynthesis at the ocean surface, and transported as sinking particles or as dissolved organic matter to the deep ocean. Remineralization converts organic matter back into dissolved inorganic matter deep in the ocean.

This biological process, called the **soft-tissue pump** [Volk and Hoffert, 1985], leads to a net transport of inorganic carbon from surface to depth. Another mechanism important in the ocean is the formation and dissolution of calcite and aragonite associated with coccolithophorids and foraminifera:



Equations 1 and 2 show that the formation of mineral calcium carbonate shells at the sunlit surface is associated with a decrease in both *DIC* and *ALK*, while dissolution of CaCO_3 shells deeper in the water column results in an increase in *DIC* and *ALK*. Due to the double charge of the carbonate ion, the formation and dissolution of calcium carbonate changes *ALK* twice as much as it changes *DIC*. The net effect is therefore a transfer of *ALK* and *DIC* to depth in a 2:1 ratio, a process called the **carbonate pump** [Volk and Hoffert, 1985]. The soft-tissue and carbonate pumps add up to the full **biological pump**.

Carbon dioxide is more soluble in cold water than in warm water. Colder deep waters are therefore expected to hold more *DIC* than warmer surface waters. Both the North Atlantic and the Southern Ocean are areas of deep water formation. Here, cold high latitude surface waters rich in *DIC* are submerged to the deep creating the Antarctic bottom water (AABW) and the North Atlantic Deep water (NADW). The NADW penetrates southward at depths between 1500 m and 2500 m, as an essential part of the oceanic thermohaline circulation (THC). The AABW penetrates to the north along the bottom in all ocean basins. This circulation pattern results also in a net increase in *DIC* at depth relative to the surface. The net transport of carbon from the surface of the ocean to the deep which is due to temperature and salinity effects only is called the **solubility pump**. We will show that the *DIC* gradient between the surface and deep ocean in the absence of biology is indicative of the strength of the **solubility pump**. Simple box models show that without the biological and solubility pumps, $p\text{CO}_2_{atm}$ would increase to ~ 420 ppm, 50% higher than its pre-industrial value [Marinov *et al.*, in prep.].

1.1 THE REPRESENTATION OF OCEANIC CARBON PUMPS IN BOX MODELS

Using the simplest representation of the biological pump in the context of a two box model of the ocean with a surface and a deep box (Figure 1), the equation for the deep ocean balance of PO_4 can be written as:

$$V_d \frac{\partial \text{PO}_{4d}}{\partial t} = \nu \cdot (\text{PO}_{4s} - \text{PO}_{4d}) + \Pi_{\text{PO}_4} \quad (4)$$

where ν is a vertical exchange rate in m^3/s , PO_{4s} and PO_{4d} are the surface and deep phosphate concentrations in mol/m^3 , and V_d is the volume of the

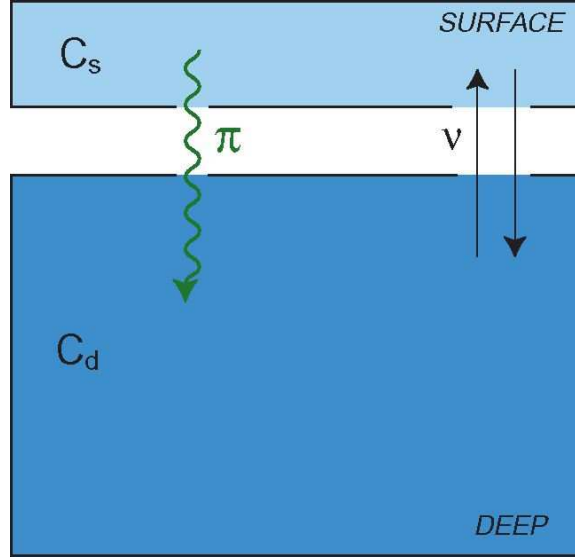


Figure 1. The two-box model representation of the oceanic biogeochemical loop. C_s and C_d are surface and deep concentrations, respectively. Π (mol/yr) is the biological pump, while ν (m^3 /yr) is the vertical exchange rate between the reservoirs.

deep ocean in m^3 . The net biological export production is represented by the sinking particle and dissolved organic matter flux Π_{PO_4} measured in mol/s of PO_4 . Here, the time rate of change of deep PO_4 depends on the surface to deep concentration difference, which increases as more organic matter falls to the deep and gets remineralized back into inorganic PO_4 . Biological production consumes PO_4 and DIC , and produces O_2 at the surface. In the interior of the ocean, organic matter remineralization consumes O_2 , and produces inorganic PO_4 and DIC . All these processes tend to occur in constant “stoichiometric” ratios of $C:P:O_2 = 117 : 1 : -170$ [Anderson and Sarmiento, 1994]. Writing Eq. 4 at steady state for O_2 , PO_4 and DIC yields

$$\begin{cases} \nu \cdot (PO_{4d} - PO_{4s}) = \Pi_{PO_4} \\ \nu \cdot (O_{2d} - O_{2s}) = \Pi_{O_2} \\ \nu \cdot (DIC_d - DIC_s) = \Pi_{DIC}, \end{cases}$$

such that

$$DIC_d - DIC_s = r_{C:P} \cdot (PO_{4d} - PO_{4s}). \quad (5)$$

$$O_{2d} - O_{2s} = r_{O_2:P} \cdot (PO_{4d} - PO_{4s}), \quad (6)$$

where $r_{C:P}$ is the stoichiometric ratio of total carbon to phosphate, which also takes into account the carbon in $CaCO_3$. Plugging in mean ocean values of 234

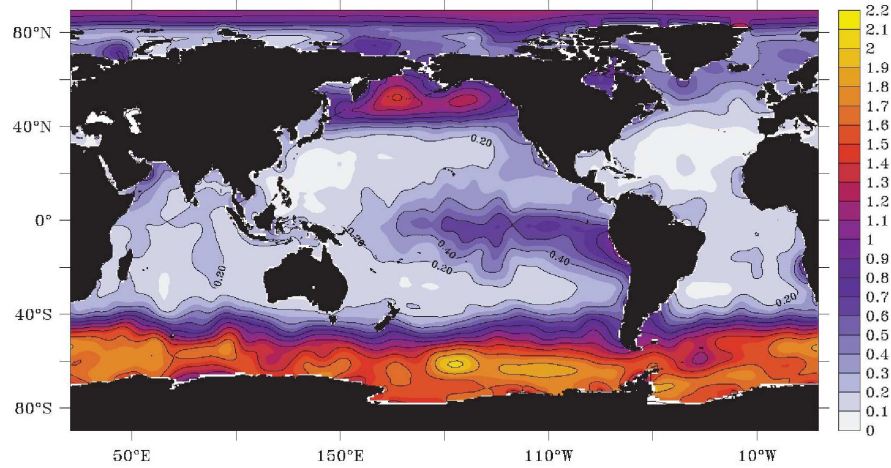


Figure 2. Observed annual mean surface phosphate at the ocean surface, in $\mu\text{mol}/\text{kg}$. From NOAA NESDIS [1994].

mmol/m^3 for O_2 , $2.1 \text{ mmol}/\text{m}^3$ for PO_4 and $0 \text{ mmol}/\text{m}^3$ for PO_4 , and using $r_{\text{O}_2:\text{P}} = -170$ [Anderson and Sarmiento, 1994] yields anoxic bottom waters with oxygen concentrations of $-123 \text{ mmol}/\text{m}^3$. This result is clearly wrong. Ocean data show deep oxygen concentrations around $170 \text{ mmol}/\text{m}^3$. Where does the two box model go wrong ?

The limitation of the two box model is related to the fact that most water that participates in the formation of deep water originates in small surface regions of the high latitudes and therefore has properties different from the global surface mean. In particular, high latitude waters are characterized by cold temperatures resulting in higher than average O_2 and inefficient biology resulting in large quantities of unutilized nutrients ($1.3 \text{ mmol}/\text{m}^3$ of PO_4), also called **preformed nutrients**. Figure 2 shows that nutrients in high latitudes are much higher than average low latitude nutrients. Because of the large scale ocean thermohaline circulation (THC), average nutrient concentrations of the high latitude surface waters feeding the deep ocean provide more appropriate values for the above problem. We modify our model to account for polar surface waters by including a third, high latitude box in our calculation, as shown in Figure 3. The atmosphere is represented by a single box with uniform $p\text{CO}_2$ of 280 ppm. The steady-state balance for O_2 , PO_4 , and DIC in the deep box becomes:

$$(\text{PO}_{4d} - \text{PO}_{4h}) \cdot (T + f) = (\Pi_l + \Pi_h) \quad (7)$$

$$(\text{O}_{2d} - \text{O}_{2h}) \cdot (T + f) = (\Pi_l + \Pi_h) \cdot r_{\text{O}_2:\text{P}} \quad (8)$$

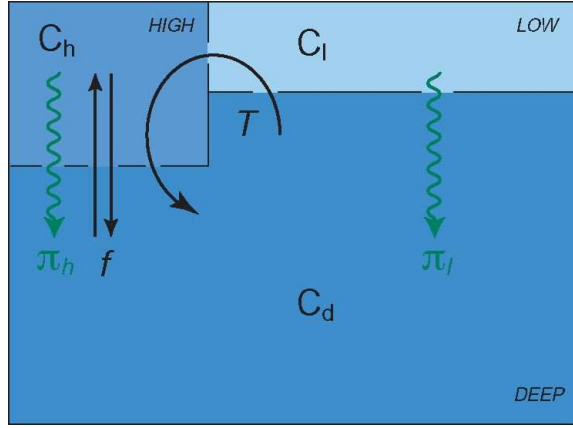


Figure 3. The three-box model of Sarmiento and Toggweiler [1984]. Box h represents the surface polar ocean of both hemispheres, box l the low and mid latitude surface ocean, box d the deep ocean. Photosynthesis converts phosphate into sinking particles, with Π_h and Π_l the measure of this export production. T is the unidirectional thermohaline overturning circulation represented as an advection process, while f is a diffusive mixing term. Both high and low latitudes exchange CO_2 with the atmosphere (not shown). Similar models were proposed independently by Knox and Mc Elroy [1984] and Siegenthaler and Wenk [1984].

$$(DIC_d - DIC_h) \cdot (T + f) = (\Pi_l + \Pi_h) \cdot r_{\text{C:P}} \quad (9)$$

where h and l represent the high and low latitude boxes, respectively. Note that in this model, export production includes both low (Π_l) and high latitude (Π_h) production. Here, T (m^3/s) represents the conveyor belt circulation, an advection process which moves water up from the deep box into the low latitude surface, poleward to high latitudes and back to the deep box. The diffusion term f (m^3/s) mixes deep and high latitude surface waters. Equations 7 and 8 give:

$$O_{2d} = O_{2h} + r_{\text{O}_2:\text{P}} \cdot (\text{PO}_{4d} - \text{PO}_{4h}) = 316 - 170 \cdot (2.1 - 1.3) = 180 \text{ mmol}/\text{m}^3, \quad (10)$$

close to the observed value of deep oxygen. This result confirms the intuition gained from our analysis of the failure of the two box model.

The low and high latitude $p\text{CO}_2$ concentrations are connected through gas exchange with the atmosphere. The steady state balance in the low latitude surface box takes into account this gas exchange:

$$(\text{PO}_{4d} - \text{PO}_{4l}) \cdot T = \Pi_l \quad (11)$$

$$(DIC_d - DIC_l) \cdot T + k_l \beta_l A_l \cdot (p\text{CO}_{2a} - p\text{CO}_{2l}) = r_{\text{C:P}} \cdot \Pi_l, \quad (12)$$

$$k_l \beta_l A_l \cdot (p\text{CO}_{2a} - p\text{CO}_{2l}) = k_h \beta_h A_h \cdot (p\text{CO}_{2h} - p\text{CO}_{2a}) \quad (13)$$

Here, k_l and k_h are gas exchange rates (m/s) representative of the low and high latitudes, respectively; A_l , A_h are ocean areas (m²) effectively exposed to gas exchange; and β_l , β_h are solubilities of CO₂ (mol/(m³·μatm)), which depend on local temperature and salinity.

In the course of this chapter we will explore different ways of measuring the strength of the biological pump. Perhaps the simplest way of thinking about the strength of the biological pump is as the *DIC* gradient between deep ocean and the high latitude box. Combining Eqs. 7 and 9 gives:

$$DIC_d - DIC_h = r_{C:P} \cdot (PO_{4d} - PO_{4h}). \quad (14)$$

The total strength of the carbon pump has a significant impact on pCO_{2atm} , by determining how much carbon is stored in the deep ocean relative to the surface ocean and the atmosphere. An increase in the carbon pump means that more carbon is sequestered in the deep ocean which will decrease pCO_{2atm} . Concretely, we see that a decrease in PO_{4h} , an increase in PO_{4d} or an increase in $r_{C:P}$ in Eq. 14 increase the biological pump strength $DIC_d - DIC_h$. Since the deep ocean is a huge reservoir, DIC_d is difficult to change. An increase in $DIC_d - DIC_h$ therefore implies a reduction in DIC_h and thus a decrease in pCO_{2h} , which allows more atmospheric CO₂ drawdown.

Since PO_{4d} is basically set by the total amount of PO_4 in the system, which is assumed constant for our purpose, Eq. 14 tells us that the strength of the biological pump is directly related to the amount of PO_4 that goes unutilized in the high latitudes, i.e., the **preformed phosphate** (PO_{4h}). A decrease in preformed nutrients strengthens the biological pump; the maximum pump strength is achieved when preformed PO_4 is zero as in the 2 BM. It is clear now that the anoxic bottom waters in the 2 BM are due to an unrealistically strong biological pump. Using a preformed value of 1.3 mmol/m³ in a 3 BM yields a lower biological pump and a realistic bottom oxygen (Eq. 10). Equations 7 and 11 yield an expression for PO_{4h} :

$$PO_{4h} = \frac{PO_{4d} \cdot f - \Pi_h + PO_{4l} \cdot T}{f + T}. \quad (15)$$

In comparison to the two box model where surface nutrients are fixed (Eq. 5), changes in T , f and Π_h can change the preformed nutrient concentration, the strength of the biological pump and therefore pCO_{2atm} . These parameters confer upon the three box model additional degrees of freedom compared to the two box model, allowing the carbon cycle to respond to glacial-interglacial changes.

1.1.1 The biological pump: glacial-interglacial changes. One of the most interesting problems in the study of climate is the attempt to understand

the glacial-interglacial cycles, characterized by significant - about 80 ppm- and fairly regular variations of atmospheric CO_2 , as seen in the Vostok ice core [Petit *et al.*, 1999].

Sarmiento and Toggweiler [1984], Knox and Mc Elroy [1984], and Siegenthaler and Wenk [1984] used simple box models in an attempt to explain the decrease in $p\text{CO}_{2\text{atm}}$ in glacial times compared to interglacials. Since changes in the solubility pump due to colder temperatures account for only 25% of the 80 ppm drop during each of the glacial periods [Bacastow, 1996] and much of this is compensated by a corresponding salinity increase [Broecker, 1982], it has been suggested that an increased biological pump strength played the principal role in lowering $p\text{CO}_{2\text{atm}}$ in glacial times [e.g., Sigman and Boyle, 2000]. Equations 14 and 15 allow many alternatives for achieving an increase in biological pump strength during glacial times, as listed below:

1.) Sarmiento and Toggweiler [1984], Knox and Mc Elroy [1984] and Siegenthaler and Wenk [1984] proposed that a decrease in preformed high latitude phosphate occurred during glacial times. According to Eq. 14 this would result in a stronger biological pump which sequesters more carbon in the deep ocean and draws more atmospheric CO_2 into the ocean. But why should we expect a decrease in high latitude surface nutrients during glacial times? Two separate mechanisms could be responsible for increased utilization of available nutrients during glacials.

1a.) An increase in the downward organic flux Π_h would increase PO_{4h} according to Eq. 15. Toggweiler *et al.* [Part 2, 2003] illustrate this mechanism in Figure 4 where a ten fold increase in Π_h more than doubles the surface to deep DIC gradient. The maximum strength of the biological pump is achieved when $\text{PO}_{4h} = \text{PO}_{4l} = 0$ and $f = 0$, i.e., when the three box model becomes a two box model. An explanation offered for the increases in high latitude productivity during glacial times is the Martin *et al.* [1990] iron fertilization mechanism. Iron concentration is relatively low in the ocean, and particularly scarce in certain nutrient rich areas (so-called high nutrient low chlorophyll or HNLC regions) such as the Southern Ocean. Martin *et al.* proposed that the growth of Southern Ocean phytoplankton is physiologically limited by the lack of iron in the present climate. Due to colder, drier, and windier climate, the atmosphere transported much more iron-bearing dust to the oceans during the last glacial maximum. This addition of soluble iron to the Southern Ocean might have increased photosynthetic uptake of CO_2 and nutrients from the surface ocean, thus increasing CO_2 uptake during glacials.

1b.) Another possible explanation for the low PO_{4h} stemming from the original BM analyses is an increase in polar stratification and the resulting reduction in Southern Ocean convective mixing f during glacial times. Consider a model in which solubility effects due to varying surface temperature and salinity are neglected. In such a model the gas exchange and distribution

of CO_2 is due only to biology and f mixes high latitude surface waters with deep waters rich in DIC and nutrients. Due to insufficient biological uptake relative to the vertical supply of carbon in the high latitudes, carbon stored in the deep ocean is thus outgassed to the atmosphere through the high latitude surface box. A decrease in f during glacial times would therefore act as a cap on the biological outgassing of CO_2 to the atmosphere in high latitudes. More CO_2 would stay in the ocean and atmospheric CO_2 concentration would decrease. This mechanism was systematically analyzed by *Toggweiler* [1999] in the context of 3, 4, 6, and 7 box models.

2.) Another possible mechanism for lowering $p\text{CO}_2\text{ atm}$ stemming from Eq. 14 is to change the total oceanic inventory of DIC and therefore DIC_d , which could be feasible by changing the total carbon inventory in land plants. *Shackellton* [1977] shows, however, that this mechanism works in the opposite direction. *Broecker* [1982] suggested that a change in the deep ocean inventory of PO_4 due to PO_4 dissolution from exposed shelves was responsible for the observed glacial-interglacial difference in $p\text{CO}_2\text{ atm}$. This mechanism was however shown to result in a delay of the CO_2 change well beyond what is observed in trapped air-bubbles in ice cores [*Sigman and Boyle*, 2000].

Others contend that fixed nitrogen rather than phosphorus limits the net effect of the biological CO_2 pump on geologic timescales and that the ratio of N fixation/ denitrification plays a key role in establishing atmospheric CO_2 [*McElroy*, 1983; *Falkowski*, 1997]. Nitrogen is involved in photosynthesis and remineralization just like phosphorus. Additionally, bio-available oceanic nitrogen is supplied through river input, rain, and in situ fixation, and is lost from the ocean through denitrification. If nitrogen limits biological production, an increase in its oceanic inventory during glacial times would have stimulated the production of phytoplankton, contributing to the observed decrease in $p\text{CO}_2\text{ atm}$. This could have been brought about by a decline in denitrification during glacials [*Ganeshram et al.*, 2002], increased continental weathering, or enhancement of nitrogen fixation by increased aeolian fluxes of iron [*Falkowski*, 1997].

3.) It is possible that physical processes such as stratification and mixing dictate ecosystem structure. Since some species do better in certain environments than others, the bulk stoichiometric ratio of carbon to phosphate $r_{\text{C:P}}$ might change if we alter the physics of the environment, thus changing the biological pump (Eq. 14). At the same time we note that the stoichiometric coefficient $r_{\text{C:P}}$ depends on the fraction of biological production going into the formation of CaCO_3 , which might have changed between glacials and interglacials. Mechanisms based on changes in the carbonate cycle might have played some part in the glacial-interglacial changes in biological pump; these are discussed by *Archer and Maier-Reimer* [1994].

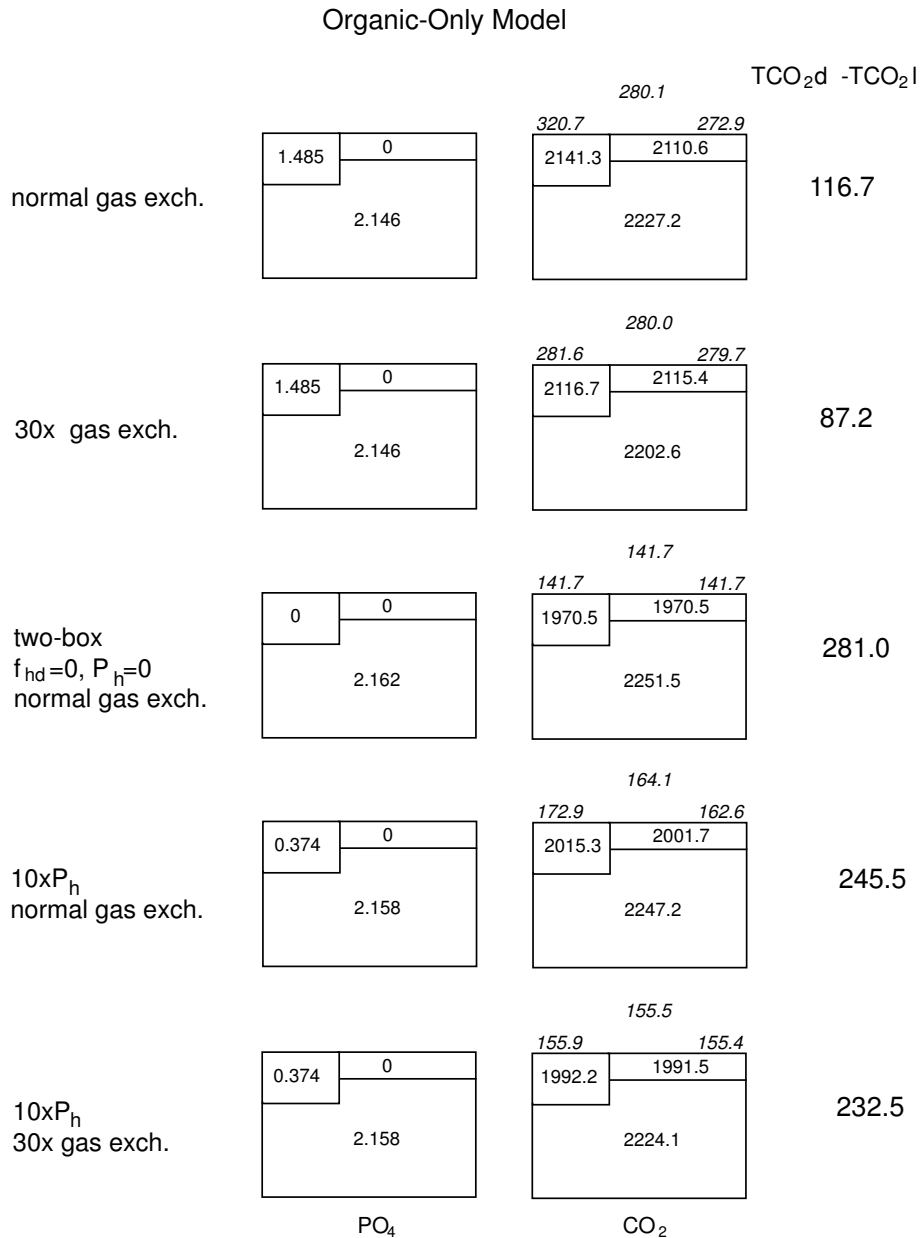


Figure 4. Figure 2 of *Togweiler et al.* [Part 2, 2003]. PO_4 , DIC , pCO_2 concentrations, and $DIC_d - DIC_l$ (here $TCO_2d - TCO_2l$) for five solutions of a soft-tissue only model. Standard simulations have $T=20$ Sv and $f_{hd}=60$ Sv (f in this paper). PO_{4l} is set to zero. The top two panels give results from the 3BM with normal and fast gas exchange; the bottom two panels give results from a ten fold increase in export production, P_h (Π_h in this text). Total amount of CO_2 in normal gas exchange models (panels 1, 3, 4) is kept constant to the amount given in panel 1; total amount of CO_2 in fast gas exchange models (panels 2, 5) is kept constant to the amount given in panel 2. An increase in export production or a decrease in gas exchange increase the biological pump strength, as measured by the DIC gradients in italics, and as shown in our analysis in Section 2.1.

1.1.2 The biological pump: the effect of surface disequilibrium. Recently, a series of papers have been written proposing that gas exchange disequilibrium in the high latitudes of the Southern Ocean may play an important role in the glacial-interglacial cycle of atmospheric CO₂. We discuss here how one can use the box models to gain insight into how this functions.

Volk and Hoffert [1985] first proposed the average low latitude surface-to-deep gradient of *DIC* in the ocean, $DIC_d - DIC_l$, as the relevant metric for the strength of the carbon pumps. We rewrite Eqs. 11- 13 as:

$$DIC_d - DIC_l = r_{C:P} \cdot (PO_{4d} - PO_{4l}) + dC_{gasex}, \quad \text{where} \quad (16)$$

$$dC_{gasex} = -k_h \beta_h A_h \cdot (pCO_{2h} - pCO_{2a})/T. \quad (17)$$

Equation 16 suggests that another mechanism potentially responsible for the increase in strength of the biological pump during glacial times is a change in the degree of equilibration of surface waters with atmospheric CO₂, dC_{gasex} . Consider a scenario in which either the thermohaline circulation (T) is strong, the gas exchange rate (k_h) is low, or the effective gas exchange area (A_h) is small. In such a scenario, water sinking into the Southern Ocean has less time to equilibrate with the atmosphere by outgassing carbon dioxide, and as a consequence deep water ends up trapping more *DIC* than the equivalent watermass in a scenario where these parameters are reversed in magnitude. This increases the total storage of CO₂ in the deep ocean. In terms of our equations, note that in a biology only scenario $pCO_{2h} > pCO_{2a}$ and $dC_{gasex} < 0$ (Eq. 17). Decreasing k_h or A_h or increasing T thus increase the strength of the biological pump as given by Eq. 16 and as illustrated graphically in the top two panels of Figure 4 from *Toggweiler et al.* [Part 2, 2003].

This mechanism is equivalent to the sea-ice mechanism proposed by *Stephens and Keeling* [2000], and the gas exchange mechanism of *Toggweiler et al.* [Part 2, 2003]. Interestingly, this mechanism occurs also as a result of self-sustained climate oscillations in *Gildor et al.* [2002]. Increased sea ice coverage decreases A_h and results in a decrease in gas exchange efficiency in high latitudes, and therefore a stronger biological pump. *Stephens and Keeling* [2000] conjecture that complete coverage with ice of the Southern Ocean during glacials would have decreased atmospheric pCO_2 by 80 ppm relative to the present CO₂ level. For more on this and other glacial-interglacial mechanisms see also the Chapter 10, “Glacial-Interglacial Cycles” in this book.

1.2 THE REPRESENTATION OF CARBON PUMPS IN GCMS AND THE EFFECT OF THE PUMPS ON AIR-SEA CARBON FLUXES

The distribution of carbon in the ocean is affected by both the biological and the solubility pumps, which depend in turn on the detailed circulation charac-

teristics and gas exchange at the surface. General circulation models (GCMs) offer us a closer, more detailed look at what sets the strengths of these pumps in the ocean. GCMs also enable us to examine another important aspect of the global carbon cycle, namely, what sets the pattern of CO₂ flux at the surface of the ocean.

The ocean circulation model we will use for illustration in this chapter is the Modular Ocean Model, Version 3 in the exact setup described by *Gnanadesikan et al.* [2002]. The biogeochemical component of the model follows the OCMIP2 specifications [Najjar and Orr, 1999]. The model includes surface production and sub-surface consumption of organic phosphorus, carbon and oxygen in a ratio of P:C:O₂ = 1:117:-170 [Anderson and Sarmiento, 1994], carbon chemistry and physical transport of nutrients and *DIC*. Dissolved organic phosphate and calcium remineralization follow prescribed functions of depth. Biological production of organic phosphorus J_{Prod} (mol/m³/s) occurs only in the euphotic layer (top 75 m) and is given by:

$$J_{Prod} = 1/\tau \cdot (PO_4 - PO_4^*) \quad \text{if } PO_4 > PO_4^* \quad (18)$$

$$J_{Prod} = 0 \quad \text{if } PO_4 < PO_4^*. \quad (19)$$

In our standard run, PO₄ is restored to the observed (Levitus) surface nutrients, represented by PO₄^{*}, with $\tau = 30$ days. The air-sea gas transfer of CO₂ in the model follows the standard formulation of *Wanninkhof* [1992] which can be written in a simplified manner as:

$$Flux = k \cdot \beta \cdot (pCO_{2\ ocean} - pCO_{2\ atm}), \quad (20)$$

where k is a gas transfer coefficient (m/s) which is a function of wind speed, Schmidt number, and sea ice fraction and β is the CO₂ solubility (mol/m³·μatm). $pCO_{2\ ocean}$ is the partial pressure at the surface of the ocean computed at each time step from prognostic variables of the model: temperature (T), salinity (S), *DIC*, and *ALK*.

Four different simulations will be presented in this section. Three simulations illustrate the impact of changing gas exchange or sea ice coverage on the air-sea flux, by analogy with the box model mechanisms presented in Section 1.1.1. In these simulations the model is run to equilibrium with a preindustrial $pCO_{2\ atm}$ of 278 ppm. A fourth simulation show the impact of driving PO_{4_h} to zero in the Southern Ocean, by analogy with mechanism 1, Section 1.1.1. In this case the model is run to equilibrium while keeping the total ocean-atmosphere carbon budget fixed.

The air-sea flux of CO₂ can be separated into a solubility component due to the solubility pump and a biotic component due to the biological pump. The solubility component is mainly a consequence of the heat and water fluxes, which change the solubility of carbon and lead to locally large air-sea CO₂

fluxes. The biological formation of dissolved and particulate organic carbon and calcium carbonate and the transport of these materials to other regions of the world where they are remineralized or dissolved leave their imprint on the biological component of the carbon flux. We separate the two effects by running two separate models.

In a first **biology only model** we turn the solubility pump off by setting the ocean temperature and salinity constant everywhere at the surface in the calculation of the air-sea gas exchange of CO_2 [Toggweiler *et al.*, Part 2, 2003; Marinov *et al.*, in prep.]. The values chosen for T and S are observed average surface values of 10°C and 34.7 psu, respectively. Our model includes both the carbonate and soft tissue pumps.

The biological air-sea CO_2 flux is intrinsically related to the nutrient distribution at the ocean surface, PO_4^* , shown in Figure 2. In high surface nutrient concentration regions such as the Southern Ocean, North Atlantic, and North Pacific, biological uptake J_{Prod} is inefficient relative to the upward supply of excess carbon and nutrients. Consider the Southern Ocean, a region of strong upwelling of deep waters characterized by the largest amount of preformed nutrients. Here J_{Prod} is not strong enough to take up all of the PO_4 from the surface water. As remineralized nutrients and CO_2 upwell, the $p\text{CO}_2$ at the ocean surface builds up, resulting in the escape of CO_2 to the atmosphere.

In a steady state, large uptake in the subtropics is required in order to counterbalance high latitude degassing. While the subtropics are overall a CO_2 uptake region, waters high in nutrients and DIC are brought up by upwelling along the coast of NW South America, in the sub-Arctic Western Pacific, Equatorial Eastern Pacific and by the upward entrainment of the equatorial undercurrent water, contributing locally to large biological CO_2 fluxes out of the ocean.

In a second **solubility model** biology is turned off [Murnane *et al.*, 1999]. The air-sea flux of CO_2 is the result of changes in CO_2 solubility due primarily to heat fluxes and to a smaller extent to water fluxes. Warming of relatively cold upwelled water in equatorial regions decreases gas solubility and results in loss of CO_2 to the atmosphere. This loss is offset by the gain of CO_2 in high latitudes due to cooling of the surface waters. Solubility effects generally oppose the effect of the biology on the air-sea flux. Figure 5 shows the strong **compensation** between the biological (starred line) and solubility air-sea flux (dashed line).

Finally, a **full model** which includes both biological and solubility effects is run. The full air-sea CO_2 flux represented by the full line in Figure 5 is very well approximated by the sum of the biological and the solubility air-sea fluxes (dotted line). Carbon cycle models do a reasonable job at reproducing the observed spatial distribution of the pre-industrial air-sea CO_2 flux. Indeed, our full CO_2 flux is very similar to the flux estimated from observa-

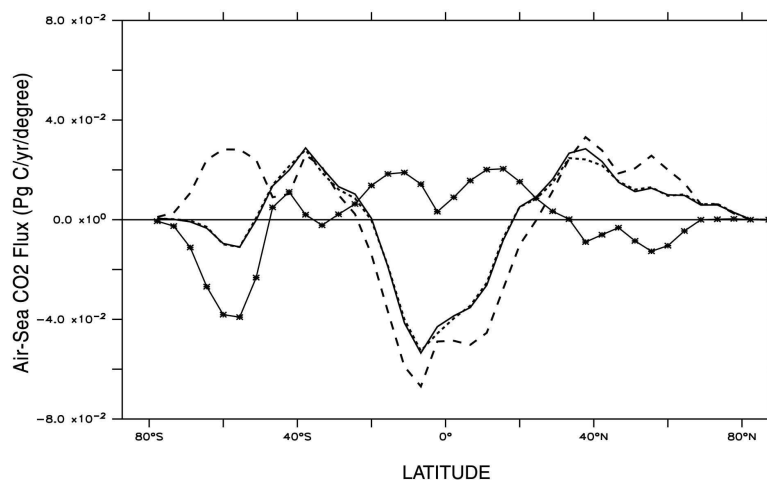


Figure 5. Equilibrium air-sea DIC flux components from a set of Princeton MOM3 simulations (PgC/yr/degree). The starred and dashed lines are air-sea fluxes from biology only and solubility only models, respectively. The dotted line is the sum of these two, while the full line is the total flux from a standard pre-industrial run which includes both biology and solubility effects. All models were run to equilibrium with a fixed atmosphere of 280 ppm. The standard full run (full line) is the so-called “LL” run of *Gnanadesikan et al.* [2002].

tions by *Takahashi* [1999] shown in Figure 6. This is to be expected since in our model nutrients, temperature, and salinity are restored towards observations at the surface of the ocean.

In order to explore analogies with the box model we calculate the surface to deep DIC gradients in the solubility, biology only, and full models. Since the DIC of the waters feeding the deep ocean is hard to determine exactly in GCMs, we express our carbon pumps by analogy with the $DIC_d - DIC_l$ metric proposed in Section 1.1.2. DIC gradients here are calculated as deviations from the corresponding mean surface DIC concentration, such that all surface values are in each case zero. Figure 7a shows that the sum of the solubility only and biology only DIC gradients (dotted line) is an excellent approximation to the full model DIC gradient (full line). The difference between the dotted and full lines is due to nonlinearities in the carbon chemistry. For example, the addition of biology to a solubility model changes the surface chemistry, modifying the response of the system to addition or removal of heat.

The biological pump and the corresponding air-sea flux depend strongly on the preformed nutrients and the efficiency of gas exchange, as suggested by our discussion in Section 1.1.2. Figure 7b shows results from the biology only model in which we have either increased the gas exchange, or we have depleted surface nutrients in the Southern Ocean. We discuss each of these in turn.

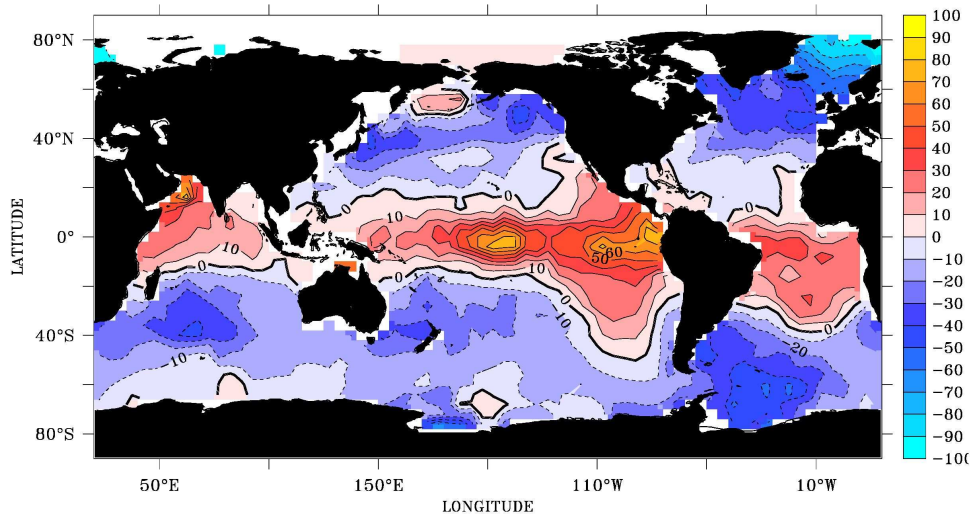


Figure 6. Annually averaged CO_2 flux at the ocean surface in $\text{mol}/\text{m}^2/\text{yr}$ for year 1995. Estimated from measurements of sea-air $p\text{CO}_2$ difference by Takahashi *et al.*, [1999].

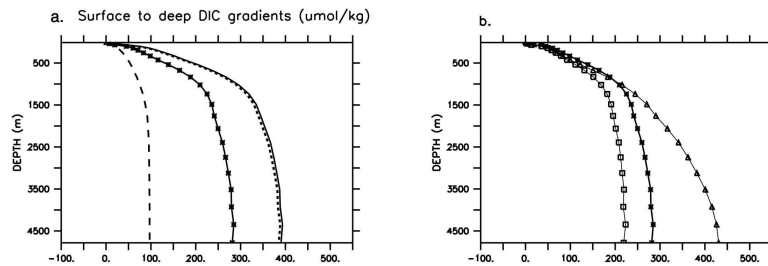


Figure 7. a. Gradients in DIC from our set of Princeton GCM simulations: a solubility only model (dashed line), a biology only model (starred line) and a full model with biology and solubility effects (full line). The sum of the latter two (dotted line) is a good approximation to the DIC gradient in the full model (full line). b. DIC gradient from a biology only model with normal gas exchange (starred line), infinitely fast gas exchange (squares), and normal gas exchange after Southern Ocean nutrient depletion south of 30°S (triangles). The normal gas exchange model is the same one used for Figure 5.

In a first simulation with the biology only model we set the gas exchange to be as fast as possible by requiring surface DIC values at the ocean surface to be in equilibrium with the overlying atmosphere at each time step. Increasing gas exchange means that more of the deep CO_2 escapes to the atmosphere through the high latitude surface waters. The result is a net decrease in the surface-to-deep DIC gradient and therefore in the strength of the biological

pump compared to the standard biological run. This mechanism is analogous with those observed in box models and discussed in Section 1.1.2 and is also shown in the top two panels of Figure 4. Incomplete equilibration of the Southern Ocean due to slower gas exchange could have contributed to a stronger biological pump and a lower atmospheric $p\text{CO}_2$ during glacials [Toggweiler *et al.*, 2003; Stephens and Keeling, 2000].

Traditionally, GCM based studies of the ice-age CO_2 drawdown focused on mechanisms that enhance the fertility of the ocean or on mechanisms that increase the ratio of organic matter relative to CaCO_3 in the sinking flux [Archer and Maier-Reimer, 1994; McElroy, 1983]. An increase in nutrient utilization in high latitudes was one of the first explanations offered for the observed decrease in atmospheric CO_2 going from interglacials into glacials (mechanism 1a., Section 1.1.1). Fertilizing the ocean with iron so as to increase biological productivity has also been proposed as a potential mechanism for offsetting anthropogenic emissions of carbon dioxide [Martin, 1991].

Assuming that the total amount of phosphate in the ocean is fixed, Equation 14 implies that the maximum gradient in DIC is achieved when high latitude nutrients are depleted, i.e., when PO_4^h is set to zero. In this case the organic pump operates at maximum efficiency, retaining the largest amount of CO_2 in the deep ocean. In the GCM we can approximate a more efficient biological pump by performing nutrient depletion simulations. We restore surface phosphate to zero in three different areas of the ocean: Southern Ocean south of 30°S , North Atlantic (30°N - 80°N), North Pacific (30°N - 67°N), and the tropical band (18°S - 18°N). According to our definition of biological productivity (Eq. 18), setting PO_4^* to zero maximizes J_{Prod} and strengthens the biological pump, which transfers CO_2 from the atmosphere to the ocean. After 500 years of simulation, the decrease of $p\text{CO}_{2,atm}$ is 63 ppm for nutrient depletion in the Southern Ocean, 15 ppm for depletion in the North Atlantic, 3.7 ppm for depletion in the North Pacific and 4.4 ppm in the tropical depletion simulation.

As areas of deep water formation, high latitude waters influence strongly the characteristics of the deep ocean. As expected from our 3 box model analysis, forcing nutrients to zero in high latitudes has a much stronger impact on the biological pump than forcing them to zero in low latitudes. The North Atlantic is a region where surface water is fed directly in the abyss. The Southern Ocean is a region where abyssal waters come to the surface with very high nutrients and DIC ; here these waters can lose much of the DIC that is added to the deep ocean by the biological pump. Because of these circulation characteristics, the potential change in the biological pump following depletion is much stronger in the Southern Ocean than in the North Atlantic. Because it is not an area of strong exchange with the deep ocean, the North Pacific is a weak sink of CO_2 under depletion.

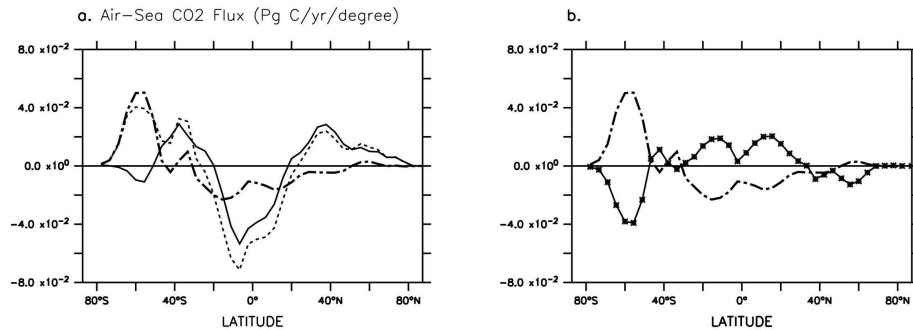


Figure 8. (a) Equilibrium air-sea fluxes of CO₂ in a full model before depletion (pre-industrial, full line) and after depletion of nutrients everywhere south of 30°S (dotted line). The difference between these two gives the dash-dotted line. Note that the air-sea flux after depletion is similar to the solubility only flux in Figure 5. (b) The contribution due to depletion (dash-dotted line) nearly cancels out the biological air-sea flux (starred line, see also Figure 5). Depletion puts the ocean in a state where there is no net air-sea flux due to biological cycling.

Figures 7b and 8 show the impact of Southern Ocean nutrient depletion on the biological pump and on the total air-sea fluxes of CO₂, respectively. Figure 8a shows the standard air-sea flux before depletion (full line, includes both solubility and biological effects), and the air-sea flux after performing nutrient depletion (dotted line). The dash-dotted line is the difference between the above two lines, and represents the change in air-sea flux due to the depletion.

Under this depletion scenario and for this particular circulation and gas exchange, the biological pump in the Southern Ocean operates at its maximum, as shown by the high *DIC* gradient in Figure 7b. Biology is highly efficient such that all the nutrients brought from the deep and the CO₂ associated with them are consumed during photosynthesis, increasing significantly the net export production. Consequently CO₂ is not allowed to escape to the atmosphere and the total biological CO₂ flux is close to zero. This is exactly the meaning conveyed by Figure 8b, which shows that the air-sea flux component due to depletion (dash-dotted line) acts in such a way as to cancel out the initial (pre-depletion) biological air-sea flux (starred line). The significant cancellation north of 30°S suggests that the Southern Ocean plays a critical role in setting up the biological pump in the rest of the ocean. Note that the total air-sea flux after depletion (dotted line in Figure 8a) is roughly equal to the pre-depletion solubility flux (dashed line in Figure 5).

Archer *et al.* [2000] made the point that different models respond differently to nutrient depletion simulations. In particular, they found that the decrease in atmospheric *p*CO₂ with nutrient depletion is considerably larger in simple box models than in GCMs.

To gain some insight into why this might be so, let us consider again Eqs. 14 and 16. While in the 3 box model there is only one type of preformed nutrient (PO_4^h), the net preformed nutrient “seen” by the deep ocean is in reality a combination of unused PO_4 from different regions of the ocean, most notably from the North Atlantic and Southern Ocean. The actual value of PO_4^h therefore depends not only on preformed PO_4 in the North Atlantic and Southern Ocean but also on the fractional composition of deep water, which is a function of advection T and mixing coefficients f characteristic to each region. Thus, different ways of representing large scale circulation, deep water formation, and mixing processes in the box models relative to the GCMs could result in different net values of PO_4^h and therefore in different responses of the biological pump to nutrient depletion. At the same time, dC_{gase} is a combination of surface disequilibrium contributions from the deep water formation regions. Recently, Toggweiler conjectured that the Southern Ocean surface water equilibrates to a different degree in box models and GCMs because of different mechanisms for deep water ventilation [Toggweiler *et al.*, Part 2, 2003]. In box models deep water is ventilated through high latitude boxes of 10% to 20% of the ocean area while in GCMs ventilation occurs in very small areas where deep convection reaches the surface. GCM surface waters are therefore far less equilibrated with the atmosphere than corresponding water masses in box models and respond less to surface nutrient depletion. Differences in surface disequilibrium can therefore be critical in explaining differences in biological pumps between box models and GCMs.

2. ANTHROPOGENIC CO_2 UPTAKE BY THE OCEANS

In order to monitor and eventually moderate climate change due to human interference on the natural system, we must understand the mechanisms driving the carbon sinks in the ocean and land, and accurately project their future evolution. The following two sections review some of the mechanisms behind the present ocean carbon sink without climate change (Section 2) and in the presence of climate change (Section 3).

The growth rate of atmospheric CO_2 , as shown in Figure 9 [Sarmiento and Gruber, 2002], was about half the rate of fossil CO_2 emissions in the 1990s. The implication is that the ocean and the terrestrial biosphere are taking out about half of the anthropogenic fossil CO_2 released to the atmosphere. Figure 9 also points to the considerable interannual variability in the total rate of uptake, which has been linked to processes such as El Niño.

Partitioning the anthropogenic carbon sink between ocean and land is a non-trivial task which has been boosted by the development of the atmospheric oxygen method of Ralph Keeling [Keeling *et al.*, 1992; Bender *et al.*, 1994;

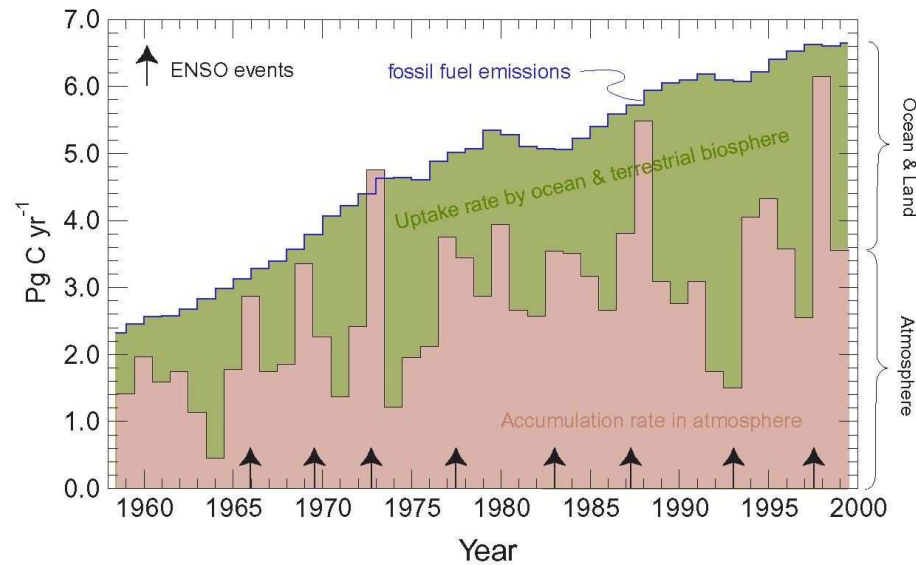


Figure 9. Growth rate of carbon reservoirs. Since 1958, the yearly accumulation rate of atmospheric carbon dioxide has grown, on average, from 1 to 3.0 Pg C/yr (light blue area). Over the same period, fossil-fuel emissions (red line) have grown from about 2.5 Pg C/yr to about 6.5 Pg C/yr. Net uptake by the ocean or terrestrial biosphere (green region) must account for the difference. Note the large interannual variation in the atmospheric CO_2 growth rate. Higher growth rates generally appear to be associated with El Niño episodes (black arrows), the exception being the period following the Mt. Pinatubo eruption in the early 1990s. Figure 3 from Sarmiento and Gruber, [2002].

Keeling *et al.*, 1996; Battle *et al.*, 2000; Manning, 2001]. More recent breakthroughs improve the global CO_2 budget by correcting for the oxygen trend due to warming of the ocean in the 1990s [Keeling *et al.*, 2002; Plattner *et al.*, 2001; Plattner *et al.*, 2002]. The resulting breakdown of carbon sources and sinks is presented in Table 1.

Uptake of CO_2 by land implies an excess of primary production over respiration and other oxidation processes such as organic matter decomposition. Land-use changes in the form of deforestation lead to a net loss of carbon from plants and soil, whereas reforestation on land that was previously farmed or logged can lead to a net gain of carbon. The exact breakdown of land carbon sources and sinks is subject to intense debate. Goodale *et al.* [2002] suggest that northern forests and woodlands provided a total sink for 0.6-0.7 Pg of C per year during the early 1990s, with most of the estimated sink in temperate forests affected by fire suppression, agricultural abandonment, and plantation forestry. Carbon may accumulate also in agricultural soils, nonforested areas responding to fire suppression, wood products both in use and in landfills, sediments of reservoirs and rivers. Pacala *et al.* [2001] suggest that the addition of

Table 1. An updated compilation of carbon sources and sinks. (a) Fossil fuel emissions and atmospheric CO₂ increase are based on the 2001 IPCC report [Houghton *et al.*, 2001]; these are our most strongly constrained estimates. (b) The land and ocean sink estimates are updated from the 2001 IPCC report to take into account changes in the O₂ method due to ocean warming [Keeling and Garcia, 2002]. These particular results are confirmed by new ocean estimates by Gloor *et al.* [2003] and McNeil *et al.* [2003]. (c) The land breakdown is very different from the 2001 IPCC report. The tropical deforestation component we show is much smaller than in the IPCC report, and is based on a recent analysis by De Fries *et al.* [2002]. The magnitude of this term continues to be controversial. The total land sink is calculated as a residual; its value is strongly debated.

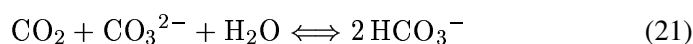
Carbon Sources and Sinks (PgC yr ⁻¹) ^a		
	1980's	1990's
Emissions (fossil fuel, cement)	+5.4±0.3	+6.3±0.4
Atmospheric Increase	-3.3±0.1	-3.2±0.1
Net Oceans/Land	-2.1±0.3	-3.1±0.4
Land and Ocean Breakdown using Oxygen and Carbon Dioxide Observations ^b		
Ocean Sink	-1.8± 0.6	-2.2±0.5
Net Land Sink	-0.3± 0.7	-0.9 ±0.7
Land Breakdown ^c		
Tropical deforestation	0.6 (0.3 to 0.8)	0.9 (0.5 to 1.4)
Total Land Sink	-0.9 (-0.6 to -1.1±0.7)	-1.8 (-1.4 to -2.3±0.7)

these terms to the forest air-to-land flux doubles the total land sink of CO₂ for the 1980-1990 decade in the US. If these non-forest sink terms were equally important everywhere else in the world, they could potentially account for the rest of the CO₂ land sink.

The net oceanic sink accounts for about one-third of the total carbon emissions, and increases between the 1980s (1.8±0.6 PgC/yr) and 1990s (2.2±0.5 PgC/yr) (Table 1). We know that the pre-anthropogenic ocean accounted for 98.5% of the total atmosphere-ocean CO₂ inventory. Why then is the oceanic uptake of anthropogenic CO₂ so small? What are the basic processes governing the uptake of excess carbon?

2.1 THE CARBONATE SYSTEM

Only one in about 20 moles of CO₂ added to the ocean stays as CO₂, while the remaining ones react with carbonate ion to form bicarbonate via the “buffering” reaction:



Following a CO_2 addition of 20 moles to the ocean, DIC increases by 20 moles while the dissolved CO_2 concentration only increases by 1 mol, such that $\partial DIC/\partial \text{CO}_2 \simeq 20$ in a pre-industrial setting. As we add anthropogenic CO_2 to the ocean, the carbonate ion concentration decreases, thus increasing the proportion of CO_2 added that stays in its dissolved form and decreasing $\partial DIC/\partial \text{CO}_2$. This results in a decrease in the overall capacity of the ocean to take up additional carbon. Carbonate buffering ensures that only 85% of the anthropogenic carbon dioxide we are adding to the atmosphere today will eventually dissolve into the ocean; this uptake capacity decreases as we put even more CO_2 in the atmosphere [Sarmiento *et al.*, 1992].

In the extreme scenario in which all of the CO_3^{2-} available today in the ocean (around 4000 GtC eq) is depleted, every mole of CO_2 entering the ocean would stay as dissolved CO_2 . In this limit at equilibrium about 33% of the added CO_2 would go into the ocean and 66% would remain in the atmosphere. On a time scale of about 10,000 years, the reaction of anthropogenic CO_2 in the deep ocean with calcium carbonate sediments accounts for a 9-15% increase in the uptake capacity of the ocean [Archer *et al.* 1998]. On even longer time scales CO_2 is neutralized by reactions with CaCO_3 and silicates on land. Because of their long time scales, these reactions have little relevance for the immediate anthropogenic uptake of CO_2 .

2.2 THE ROLE OF GAS EXCHANGE AND CIRCULATION: THE GREEN'S FUNCTION SOLUTION

In this section we assume that the natural carbon cycle is in steady state and is unaffected by the anthropogenic CO_2 addition, which we treat as a perturbation on the system. For the purpose of this section we ignore the land carbon sources and sinks. Let us consider the carbon balance for atmospheric CO_2 :

$$\frac{\partial C(t)}{\partial t} = S(t) - U(t), \quad (22)$$

where $C(t)$ is the atmospheric CO_2 concentration in ppm, $S(t)$ is the carbon input to the atmosphere at time t and $U(t)$ is the oceanic uptake at time t .

Following Maier-Reimer and Hasselmann [1987] we use a Green's Function approach to gain insight into the rate of oceanic uptake. We consider a simplified problem in which C undergoes a jump at $t = 0$, that is, $C(t) = C_o$ for $t < 0$ and $C(t) = S_o + C_o$ at $t = 0$. This corresponds to $S(t) = S_o \cdot \delta(t)$. For $t > 0$ we then seek a solution to

$$\frac{\partial C}{\partial t} = -U(t), \quad (23)$$

$$\text{with initial condition } C(0) = S_o + C_o. \quad (24)$$

In other words, we ask what is the atmospheric concentration and corresponding oceanic uptake at time t following an instantaneous addition of S_o ppm of CO_2 at time $t = 0$? In order to solve this problem we need a functional form for the oceanic uptake $U(t)$. Assuming that the ocean responds linearly to the CO_2 addition to the atmosphere, a well motivated choice is:

$$U(t) = \frac{1}{\tau} \cdot (C(t) - (C_o + A_o \cdot S_o)), \quad (25)$$

where τ is a characteristic time scale for the ocean uptake. If A_o is the fraction of the initial source pulse that stays in the atmosphere at equilibrium, $C_o + A_o \cdot S_o$ is the amount of carbon left in the atmosphere once the system reaches equilibrium and $U(t)$ decreases exponentially to 0 at equilibrium. We substitute Eq. 25 into Eq. 23 and solve for $C(t)$ subject to the initial condition (24):

$$C(t) = C_o + S_o \cdot G(t), \quad (26)$$

$$\text{where } G(t) = A_o + (1 - A_o)e^{-t/\tau}. \quad (27)$$

If there is more than one characteristic time scale for oceanic uptake τ_j , one can write the function $G(t)$ as a superposition of a number of exponentials of different amplitude A_j and relaxation time τ_j [Maier-Reimer and Hasselmann, 1987]:

$$G(t) = A_o + \sum_j A_j e^{-t/\tau_j}, \quad (28)$$

$$\text{where } A_o + \sum_j A_j = 1. \quad (29)$$

Note that A_o is associated with an infinite relaxation time scale. The Green's function $G(t)$ is the fraction of the initial source pulse still in the atmosphere at time t ; $G(0) = 1$ and $\lim_{t \rightarrow \infty} G(t) = A_o$. For an arbitrary emission function $S(t)$ the solution to Eqs. 23 - 24 can be formally written as:

$$C(t) = \int_0^t S(t') G(t - t') dt' + C_o, \quad (30)$$

where the Green's function $G(t)$ is the linear response to a pulse at time t' . Note that substituting $S(t) = S_o \cdot \delta(t)$ reduces Eq. 30 to Eq. 26, as expected.

Maier-Reimer and Hasselmann [1987] and Sarmiento *et al.* [1992] perturbed a full GCM with a step function initial change representing an instantaneous 25% increase, doubling and quadrupling of the background $p\text{CO}_2 = 280$ ppm: i.e., $S_o = 70$ ppm, 280 ppm, 840 ppm, respectively. A response of the form (26), where

$$G(t) = A_o + A_1 e^{-t/\tau_1} + A_2 e^{-t/\tau_2} + A_3 e^{-t/\tau_3} + A_4 e^{-t/\tau_4} \quad (31)$$

Table 2. Coefficients for exponential fits to the atmospheric response to a pulse input. A_j and τ_j are the amplitude and exponential relaxation time scales from Eq. 28. The numbers in the initial input column are the fraction by which the atmospheric CO₂ was increased above its pre-industrial value of 280 ppm. Table A1 in *Sarmiento et al.* [1992].

Initial Input	A_o	A_1	τ_1	A_2	τ_2	A_3	τ_3	A_4	τ_4
0.25	0.164	0.245	358.8	0.302	60.8	0.229	10.3	0.059	1.0
1.00	0.174	0.275	376.6	0.307	67.7	0.189	10.7	0.054	0.9
3.00	0.208	0.358	433.3	0.261	83.9	0.131	11.2	0.042	0.8

was least-square fitted to the atmospheric CO₂ response to a pulse input in the GCM, in order to determine A_j and τ_j . The results of one such perturbation experiment are shown in Table 2. Once $G(t)$ is determined, one can in principle use Eq. 30 to determine the atmospheric concentration given any source of excess CO₂.

In the quadrupling experiment the atmospheric concentration increase by 840 ppm represents an addition of 1780 GtC to the atmosphere, of which about 1424 GtC eventually end up in the ocean. An addition of the order 1400 GtC eq can change significantly the CO₃²⁻ reservoir, which is presently about 4000 GtC. This experiment therefore falls into a nonlinear regime in which CO₃²⁻ changes strongly and the asymptotic oceanic uptake drops accordingly to 79.2%, as contrasted with 83.6% for the 25% addition case. Though our representation of Green's functions is strictly correct only for an ocean that responds linearly to the atmosphere as in Eq. 25, the quadrupling experiment is considered in order to estimate the changes in the relaxation time scales and amplitudes due to chemical nonlinearities in the system [*Sarmiento et al.*, 1992].

The representation of the atmospheric concentration in terms of exponentials allows us to assess the importance of different physical and chemical processes on the storage of CO₂ in the ocean. The equations show that $C(t)$ is the sum of terms of the form $S_o \cdot A_j \cdot e^{-t/\tau_j}$. Each of these terms decreases exponentially as oceanic processes with time scales τ_j gradually absorb CO₂ from the atmosphere. The bigger the τ_j , the longer it takes for the particular process to absorb carbon. The time scales given in Table 2 suggest that τ_1 (350 years) is the relaxation time scale associated with deep water thermohaline circulation, τ_2 (60 years) is representative of intermediate water ventilation, τ_3 (10 years) is associated with the ventilated thermocline or gyre circulation, and τ_4 (1 year) is the time scale for the equilibration of mixed layer CO₂ with atmospheric CO₂ through gas-exchange. Thus, while on short time scales the penetration of CO₂ into the mixed layer is an important process, as t increases the absorption of CO₂ is gradually limited by larger scale circulation processes.

The coefficients A_j represent the fraction of S_o that is involved in processes with the relaxation time scale τ_j ; the sum of all the coefficients is one. Alternatively, we can think of the A_j coefficients as the relative capacities of the reservoirs j which are filled up at rates given by τ_j . Consider an initial input of 0.25×280 ppm. $A_o = 16.4\%$ is the fraction of the source that stays permanently in the atmosphere. Thus, the **potential uptake** of the ocean is $\int_0^\infty U(t) dt = S_o(1 - A_o)$, i.e. 83.6% of the added carbon dioxide. According to Table 2 on a time scale of 1 year the anthropogenic signal penetrates roughly $A_4/(1 - A_o) = 5.9/83.6 = 7.06\%$ of the total volume of the ocean; on a time scale of 10 years the signal penetrates into an additional $A_3/(1 - A_o) = 22.9/83.6 = 27.39\%$ of the ocean volume, and so forth.

Note that it is not straightforward to account for the nonlinearity of the system with the Green's function approach described above. *Maier-Reimer and Hasselmann* [1987] and *Sarmiento et al.* [1992] show that the magnitude of the A_j coefficients and the corresponding time scales τ_j depend on the size of the pulse, the initial atmospheric CO_2 concentration and the time history of the background atmospheric CO_2 . In particular, as the initial input increases, the capacity of the ocean to hold CO_2 at equilibrium goes down and more of the initial CO_2 will stay in the atmosphere, i.e., A_o increases. This general conclusion holds for more realistic scenarios in which the source function increases linearly or exponentially in time.

One can apply the Green's function method to simple box models. In a 1 BM of the ocean we can still write $G(t) = A_o + A_1 e^{-t/\tau_1}$ where τ_1 is the time scale associated with the surface gas exchange. $A_1 = 1 - A_o$ is the potential uptake of the ocean as determined by carbon buffering, i.e., approximately 85%. For the 2 BM of Figure 1 we can write $G(t) = A_o + A_1 e^{-t/\tau_1} + A_2 e^{-t/\tau_2}$, where τ_2 is the gas exchange time scale and τ_1 is the deep water ventilation time scale. τ_1 depends on the mixing between deep and surface waters ν ; large ν results in fast mixing and smaller τ_1 . The ratio of A_1 to A_2 is roughly the ratio of the bottom to the surface box volumes and $A_1 + A_2 = 1 - A_o \simeq 85\%$. *Joos et al.* [1997] explored the sensitivity of the oceanic uptake of CO_2 to different vertical diffusivity values in a box model. For a careful choice of depth-dependent diffusivity with higher values near the surface and lower values at depth, their 12 layer BM was able to reasonably predict both the uptake of anthropogenic CO_2 and natural ^{14}C observations.

We will next try to understand the role of the gas exchange in the uptake of anthropogenic CO_2 . Consider the time rate of change in the mixed layer of a gas that exchanges only with the atmosphere, such as surface oxygen O_2 *sfc*:

$$\frac{\partial \text{O}_2 \text{ sfc}}{\partial t} = \frac{1}{\tau} \cdot (\text{O}_2 \text{ atm} - \text{O}_2 \text{ sfc}). \quad (32)$$

A typical magnitude for τ can be estimated as follows:

$$\tau = \frac{z_{ml}}{k_w} = \frac{75 \text{ m}}{4 \text{ m/day}} = 18 \text{ days.} \quad (33)$$

where k_w is a gas exchange coefficient (in m/day) and z_{ml} is the mixed layer depth (in m). As the gas exchange time scale τ is very short relative to the circulation time scale, surface O_2 in water is well equilibrated with atmospheric O_2 . This is the reason why in GCMs, box models and in the real ocean the surface concentration of O_2 is very close to the O_2 saturation concentration.

The surface exchange of CO_2 is different from that of O_2 because CO_2 is a weak acid in seawater that reacts with water and carbonate (Eq. 21). The time rate of change of DIC in the surface mixed layer is well approximated by:

$$\frac{\partial DIC}{\partial t} = \frac{\partial DIC}{\partial CO_{2\ sfc}} \cdot \frac{\partial CO_{2\ sfc}}{\partial t} = \frac{k_w}{z_{ml}} \cdot (CO_{2\ atm} - CO_{2\ sfc}), \quad (34)$$

such that

$$\frac{\partial CO_{2\ sfc}}{\partial t} = \frac{1}{\tau} \cdot (CO_{2\ atm} - CO_{2\ sfc}) \text{ and} \quad (35)$$

$$\tau = \frac{\partial DIC}{\partial CO_{2\ sfc}} \cdot \frac{z_{ml}}{k_w} \simeq 20 \cdot \frac{75 \text{ m}}{4 \text{ m/day}} \simeq 1 \text{ year.} \quad (36)$$

The time scale τ corresponds to τ_4 in Table 2. The characteristic time scale on which gas exchange occurs is therefore longer for CO_2 than for O_2 by the factor $\partial DIC / \partial CO_2$. Note that as more CO_2 is added to the atmosphere this ratio decreases, thus moderately decreasing τ as shown in Table 2.

The characteristic time scale of 1 year for a 75 m top layer to reach equilibrium with the atmosphere is smaller than the time-scale of the present anthropogenic perturbation, which is roughly an exponential with an e-folding time of several decades. Surface waters thus track the atmospheric perturbation closely. *Sarmiento et al.* [1992] showed that a doubling of the gas exchange coefficient k_w increases the overall excess CO_2 uptake only moderately (11% in the Princeton GCM). This experiment confirms previous intuition gained from box models [*Siegenthaler*, 1983; *Siegenthaler and Joos*, 1992] that vertical exchange is the dominant process in limiting perturbation CO_2 flux into the ocean. Thus, intermodel differences in the rate at which deep waters are exposed to the surface and then submerged into the deep or in the convective parameterization can cause large differences between the resulting carbon uptake.

The difference between the present oceanic uptake of 40% of the total atmosphere-ocean increase (Table 1) and the potential uptake of 85% of the total excess atmosphere-ocean CO_2 is explained by the slowness of the oceanic circulation, which does not mix the new anthropogenic CO_2 signal into the

deep sufficiently fast to allow for extensive surface uptake. Slow mixing between surface and deep should continue to produce ocean uptake for several centuries after an input of anthropogenic CO_2 into the atmosphere [Siegenthaler and Hasselman, 1978; Sarmiento *et al.*, 1992]. This also means that CO_2 will continue to enter the ocean for decades or centuries even after a potential stabilization of atmospheric CO_2 ; the equilibrium time scale is of the order of hundreds of years to a thousand years. The role of circulation in the uptake of anthropogenic CO_2 is further discussed in the following section.

2.3 THE ROLE OF CIRCULATION AND MIXING: MODEL RESULTS AND OBSERVATIONS

The anthropogenic signal, which can be defined as the increase in oceanic carbon dioxide relative to the pre-industrial times, is small compared to the natural signal and requires very accurate measurements in the ocean [Sabine *et al.*, 1997]. Few time-series that allow long-term, precise measurements exist. Given the present limitations to directly estimating anthropogenic CO_2 from observations, ocean models have been one of the principal tools for quantifying air-sea fluxes and oceanic uptake of anthropogenic carbon dioxide.

Figure 10 shows typical air-sea CO_2 flux results from a 3D simulation of anthropogenic carbon uptake with the same Princeton model described in Section 1.2 and Figures 5 and 8. The anthropogenic contribution is calculated directly in models by subtracting the pre-anthropogenic air-sea flux (full line) from the greenhouse-forced air-sea flux (dotted line). By comparing Figure 10 with Figure 5 we see that the increase of atmospheric $p\text{CO}_2$ above its pre-industrial level tends to increase oceanic uptake in natural sink regions such as high latitudes and decrease the release of CO_2 to the atmosphere in natural CO_2 outgassing regions. The anthropogenic uptake by the ocean (dash-dotted line in Figure 10) is calculated as the difference between the dotted and full lines. One should bear in mind that when applied to CO_2 source (outgassing) regions, uptake of anthropogenic carbon represents an actual decrease in outgassing (of the CO_2 already present in the ocean) relative to the pre-industrial state. Reduced outgassing implies that more carbon stays in the ocean; this excess carbon dioxide is what is referred to as the **anthropogenic CO_2 contribution**.

According to models, high uptake of anthropogenic CO_2 occurs as a consequence of strong exchange with uncontaminated interior waters [Sarmiento *et al.*, 1992]. Such exchange occurs in upwelling and convective overturning areas, such as the upwelling Equatorial region, the North Atlantic, and the Southern Ocean, as reflected in the air-sea flux patterns in Figure 10.

The Southern Ocean is particularly important in this regard. As upper circumpolar deep waters with low, pre-anthropogenic CO_2 upwell to the surface

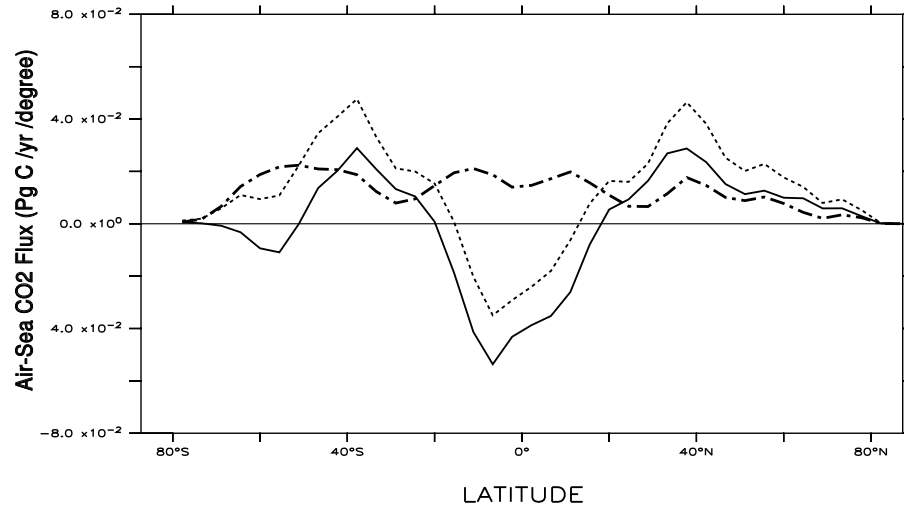


Figure 10. Anthropogenic air-sea flux of CO_2 from a standard Princeton biogeochemistry model. The model was first run to equilibrium with an atmosphere of 280 ppm while keeping the total amount of DIC in the system constant; pre-anthropogenic air-sea flux (full line) is the same as in Figure 5. CO_2 was then released into the atmosphere following the OCMIP protocol; the dotted line is the resulting air-sea flux at the present time. The difference between these two fluxes is the excess (anthropogenic) flux (dash-dotted line).

in the Southern Ocean, they interact with an atmosphere which now contains higher, anthropogenic CO_2 . Anthropogenic CO_2 penetrates this water, which is then transported northward before sinking as Subantarctic Mode Water (SAMW) and Antarctic Intermediate Water (AAIW) somewhere between 40° and 50°S [Caldeira and Duffy, 2000]. Excess carbon is thus carried to the southern subtropics, where it is stored along with CO_2 that enters the main thermocline directly in lower latitudes. This circulation pattern accounts in models for the large cumulative flux South of 40°S and for the northward shift in the total column inventory compared to the cumulative flux of anthropogenic CO_2 [Sarmiento et al., 1992].

The Ocean Carbon Model Intercomparison Project (OCMIP) is a recent effort to systematically compare different models. Participating models use identical ocean biogeochemistry and gas exchange parametrizations but different model physics (i.e, different grids, resolution, eddy mixing parametrizations). Models were forced by a spline fit to historical observations from 1765 until 1990 under prescribed, constant surface conditions (temperature, salinity, wind speed, alkalinity).

Figure 11 from Orr et al. [2001] shows the zonal mean and zonal integral of anthropogenic air-sea CO_2 fluxes in 1990 in four different OCMIP models. Significant differences in the uptake of anthropogenic CO_2 are due to different

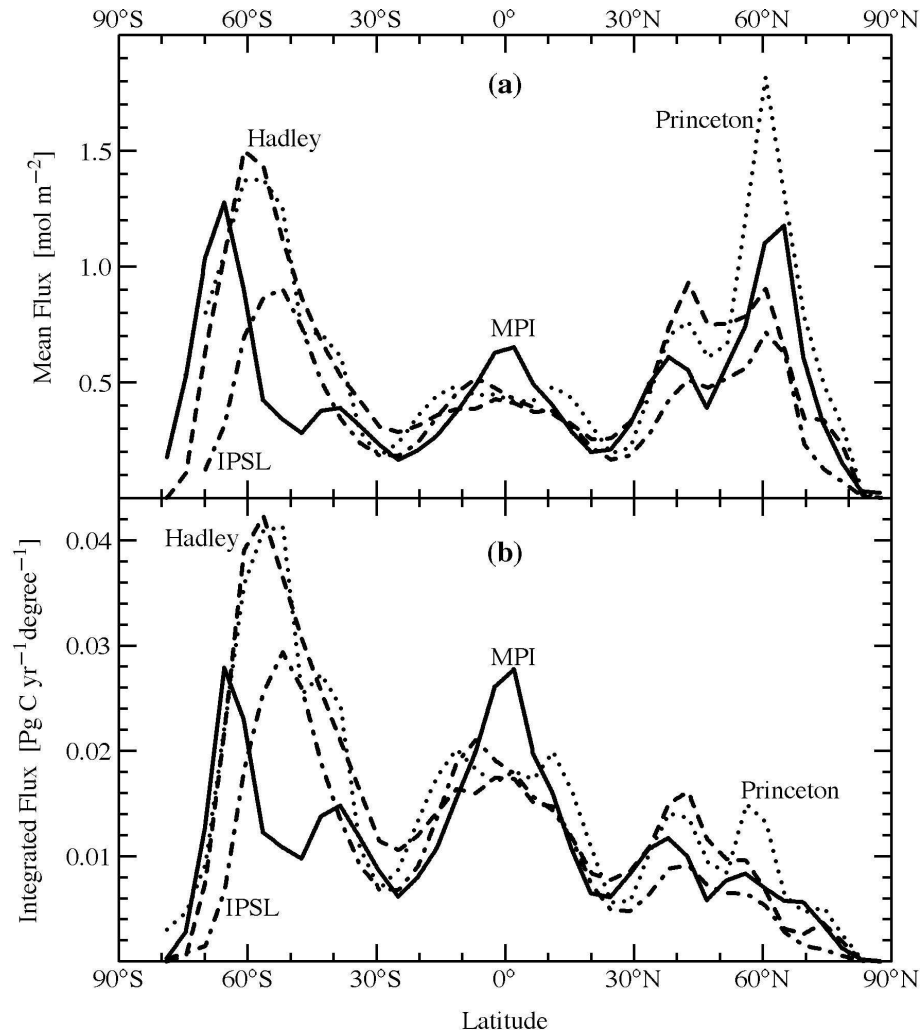


Figure 11. Zonal air-to-sea flux of anthropogenic CO₂ for the global ocean in 1990, given as (a) the zonal mean (mol/m²) and (b) the zonal integral (PgC/yr/°lat). The models compared are Hadley, MPI, IPSL, Princeton/GFDL. Figure 1 from *Orr et al.* [2001]. Note the large uptake and inter-model differences in the Southern Ocean.

physics of these models. For the MPI, IPSL, Hadley and Princeton models, flux estimates south of 30°S range from 35 to 48% of each model's global uptake. Thus, the Southern Ocean south of 30°S, with its deep wintertime mixing and strong upwelling, has higher excess carbon uptake and inventory than expected from its area of 31% of the global ocean area [*Orr et al.*, 2001]. The Southern Ocean is also found to account for about 50% of the inter-model variance, consistent with findings from sensitivity studies that this is the region with highest

variability of CO₂ uptake in response to changes in physical parametrizations [Matear, 2001; Marinov *et al.*, in prep.]. This suggests that tracer uptake in the Southern Ocean is poorly determined by models and highly uncertain.

A critical component for global carbon cycle studies is the evaluation of modeled anthropogenic carbon uptake and inventory through comparisons with tracer observations in the ocean. The tracers most used for such analyses are estimates of anthropogenic CO₂ itself, estimates of bomb ¹⁴C, and measurements of chlorofluorocarbons (CFCs). Because of the lack of pre-industrial CO₂ observations, estimating the oceanic inventory of anthropogenic CO₂ from observations has been done indirectly. Starting from the analyses of Brewer [1978] and Chen and Millero [1979], Gruber *et al.* [1996] proposed that the total anthropogenic CO₂ concentration in the ocean is given by

$$C_{anth} = C - C_{bio} - C_{eq-280} - C_{diseq}, \quad (37)$$

where C is the presently observed DIC in the ocean, C_{bio} is the contribution due to the soft tissue and carbonate pumps, C_{eq-280} is the calculated DIC equilibrium concentration with a pre-industrial pCO_2 of 280 ppm, and C_{diseq} is the DIC concentration that results from the air-sea CO₂ disequilibrium at the time the water parcel left the surface ocean. Figure 12 shows the anthropogenic DIC calculated with this method from observations of present DIC .

Anthropogenic CO₂ inventories since 1800 from models are globally in rough agreement with observational estimates. However, differences between models and observations can be large on a regional scale. Models [Orr *et al.*, 2001; Matear, 2001] seem to over-predict at high latitudes the inventory of anthropogenic CO₂ estimated from observations with the Gruber *et al.* [1996] method or with other methods [i.e., McNeil *et al.*, 2002]. Figure 12 [Gruber and Sarmiento, 2002] shows high penetration of anthropogenic CO₂ in the subtropics and low penetration into the deep Southern Ocean. Note that anthropogenic carbon has penetrated significantly below about 2000 meters of the water column only in the North Atlantic, where surface waters sink directly into the abyss. Between 50°S and 50°N CO₂ penetration is generally shallower and excess CO₂ storage is lower in models compared to data estimates. This difference between models and observations could be explained by inadequate ocean physics in the models, such as a problematic parametrization of Southern Ocean physical processes. Too much surface water ventilation in the Southern Ocean south of 50°S, for example, could lead to overestimating anthropogenic storage in the region. A northward transport out of the Southern Ocean that is too weak (due to inadequate isopycnal mixing, too low advection, or inadequate formation of SAMW or AAIW) could explain the reduced penetration and low storage in the southern subtropics in the models.

While this intercomparison points to the incomplete representation of physical processes in the GCMs, one has to also take into account the random

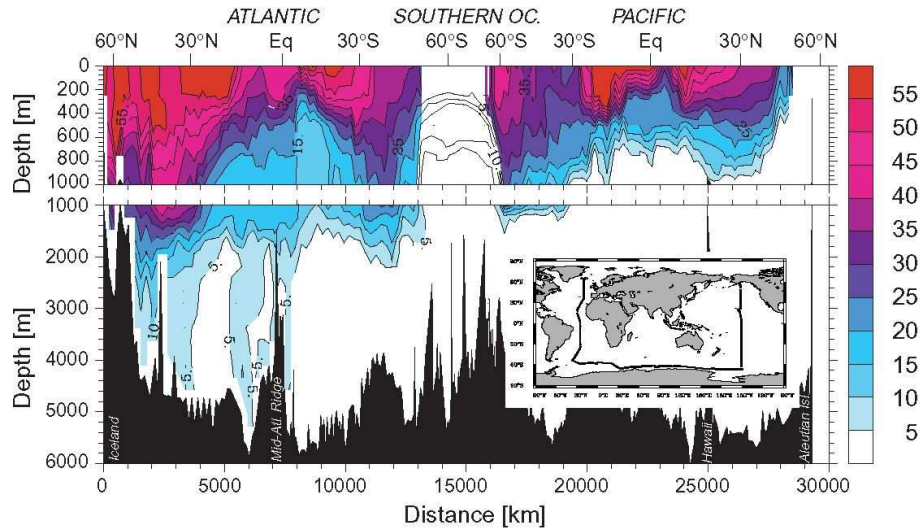


Figure 12. Anthropogenic carbon concentrations in the ocean along the track shown in the inset. The black area represents the ocean floor. The anthropogenic carbon is separated from the natural background by using the C^* method of Gruber *et al.* [1996] applied to high-precision measurements of dissolved inorganic carbon. Uncertainties in this separation technique are so large south of 60°S that they are shown there as contour lines only. Anthropogenic carbon has penetrated significantly below about 2000 meters of the water column only in the North Atlantic, where surface waters sink directly into the abyss; note the low Southern Ocean uptake. Figure 3 from Gruber and Sarmiento [2002].

and systematic errors associated with data estimation methods. For example, Coataoan *et al.* [2002] show that two studies of the same Indian Ocean data set [Sabine *et al.*, 1998 and Goyet *et al.*, 1999] using two different methods (the Gruber *et al.* [1996] method and a regression technique) produced quite different estimates for anthropogenic CO_2 storage and uptake. Therefore understanding uncertainties associated with these techniques is a much needed step, and model calibration must be principally done with tracers such as CFC s, where these uncertainties do not exist.

Since they enter the ocean via gas exchange and are transported in the ocean as passive and conservative tracers, CFC s have been proposed as “ventilation clocks” for the ocean, i.e., as indicators of water age and deep ocean ventilation. CFC -11 and CFC -12 have been proposed as analogs of anthropogenic CO_2 because they grew exponentially from 1950 to 1995 just as anthropogenic CO_2 has since the Industrial Revolution. CFC s have the advantage over an-

thropogenic CO₂ and bomb ¹⁴C that they have no natural background and they can be measured with high precision, with extended coverage from the recent World Ocean Circulation Experiment.

A number of studies have used *CFCs* to evaluate models of the ocean circulation [e.g., England, 1995; England and Hirst, 1997, Dutay, 1998, etc.], decadal scale ventilation characteristics [Dutay *et al.*, 2002], and to validate model parametrization schemes [Robitaille *et al.*, 1995]. Model sensitivity studies in which one varies the gas exchange formulation or the circulation characteristics should help us understand better the effect of these processes on relations between bomb ¹⁴C, *CFCs*, and anthropogenic CO₂ inventories. Observed tracer-tracer relations could guide our choice of appropriate gas exchange or mixing parametrizations, and lead to significant model improvement.

3. THE OCEAN CARBON CYCLE AND CLIMATE CHANGE

3.1 CLIMATE RESPONSE TO CO₂ INCREASE

Simulations of the anthropogenic CO₂ increase in atmosphere-ocean models coupled with ocean biogeochemistry have traditionally been done in models with constant oceanic circulation, sea temperature, and biology such as those analyzed in Section 2. However, all coupled climate models to date predict that continuous emissions of anthropogenic CO₂ lead to increased radiative forcing resulting in higher sea surface temperature (SST) and a stronger hydrological cycle, accompanied by significant changes in ocean circulation and mixing [IPCC report, 2001].

At present, the high latitude ocean loses heat and gains fresh water from precipitation and runoff. In simulations of greenhouse gas forcing, increased poleward transport of moisture in the atmosphere [Schiller *et al.*, 1997] results in increased precipitation in high latitudes and especially in the formation region of the NADW. In some models, this causes a freshening of high latitude waters [Manabe and Stouffer, 1993] and a strong decline in surface density, particularly in the formation regions of NADW and AABW. At the same time, increased SST further decreases surface density, stabilizing the upper column throughout the ocean (Fig. 13e). This surface stabilization reduces vertical mixing by flattening isopycnals, and diminishing convective mixing and thermohaline overturning. The relative roles of the temperature increase and of the surface freshening on surface stabilization remains controversial [Dixon *et al.*, 1999; Mikolajewicz and Voss, 2000], with some models showing that freshening in the North Atlantic is counteracted by advection of high salinity waters from the tropics [IPCC report, 2001].

All of the above changes are likely to result in a modification of the thermohaline circulation, with some models indicating a reduction in the North Atlantic maximum meridional overturning circulation (a measure of the THC) of 10%-50% following a CO₂ increase in the atmosphere up to the year 2100 [Manabe and Stouffer, 1993; Stocker and Schmittner, 1997]. Most models so far project significant changes in the marine carbon cycle and a reduction in the oceanic carbon uptake due to all of these processes, which may in turn accelerate atmospheric CO₂ growth [Sarmiento and Le Quere, 1996; Matear and Hirst, 1999; Cox *et al.*, 2000].

Of some concern is a scenario in which the entire thermohaline circulation collapses after passing a critical threshold, when the global atmospheric temperature has increased by 3.7 – 7.4°C [Manabe and Stouffer, 1993; Schmittner and Stocker, 1999; Dixon *et al.* 1999]. The reduction or shut-down of the THC leads to a reduction in the meridional transport of heat in the Atlantic, and a regional cooling which counteracts the temperature increase. The meridional distributions of precipitation and warming [Schiller *et al.*, 1997], sea-level rise [Knutti and Stocker, 2000], and biogeochemistry of the ocean [Joos *et al.*, 1999; Sarmiento and Le Quere, 1996] would all be profoundly affected by this scenario [Stouffer and Manabe, 1999].

Physical processes such as convection, diffusion and sub-grid scale (eddy) motions, while fundamental for calculating the oceanic uptake of natural and anthropogenic CO₂ (Section 2), are not resolved and are instead parameterized in climate models. Climate change predictions depend strongly on the response of the hydrological cycle to warming, the parameterization of mixing processes and of deep water formation, the vertical transport of heat, and the rate of temperature increase [Stocker and Schmittner, 1997]. Differences in the representation of these processes and our crude rendition of sea-ice processes account for large uncertainties and inter-model differences in climate warming simulations.

3.2 CO₂ RESPONSE TO GLOBAL WARMING

3.2.1 Oceanic feedbacks. The continuous release of anthropogenic CO₂ into the atmosphere changes the physical and biogeochemical properties of the oceans. A change in these properties could influence the future uptake of anthropogenic CO₂ by the oceans and therefore $p\text{CO}_2_{atm}$. The present section discusses some of these property changes, which can be either direct changes in the anthropogenic uptake itself (point 1 below), or indirect changes through alterations of the natural solubility and biological pumps in the ocean (points 2-4). For the purpose of this paper we define positive feedback as the interaction between climate change and the carbon cycle that results in an increase in $p\text{CO}_2_{atm}$ and a decrease in the ocean carbon uptake.

1. As anthropogenic CO₂ accumulates in the surface ocean, the carbonate chemistry of the ocean continuously changes. This process modifies the *carbonate buffering* and is a positive feedback acting to decrease the uptake capacity for CO₂ as more anthropogenic carbon is added to the ocean (see Section 2.1).
2. The continuous emission of CO₂ increases radiative forcing and results in a net heat flux into the ocean. Gases are less soluble in warmer waters. Warming of the surface waters therefore increases surface *p*CO₂ and drives CO₂ out of the ocean. This is a positive feedback; the chemical capacity of the ocean to dissolve anthropogenic CO₂ decreases as SST rises.
3. Coupled atmosphere-ocean models predict increases in vertical stratification and a general weakening of the vertical component of isopycnal mixing and convective overturning. As a consequence, the amount of water submerged from or upwelled to the surface changes. This slowing of vertical exchange will alter both the natural carbon cycle and the uptake of anthropogenic CO₂. Models so far predict an overall decrease in cumulative oceanic uptake of anthropogenic carbon due to circulation changes, i.e., a positive feedback (see Table 3 and discussion in this chapter).
4. Perhaps the largest unknown and the hardest to systematize are changes in the carbon uptake due to changes in ocean biology. The ocean biological pump can be affected by numerous climate-related factors such as: temperature, cloudiness or light availability, nutrient availability, ocean physics, sea-ice coverage. In a recent study, *Falkowski et al.* [1998] pointed to three factors, listed below, that could affect the strength of the biological pump and therefore the oceanic uptake of CO₂. For a more comprehensive review of these factors see also the 2001 IPCC report.
 - a. Changes in surface nutrient utilization in nutrient rich areas. Changes in the supply of iron to high nutrient low chlorophyll [HNLC] regions might affect the utilization of surface nutrients, thereby changing export production and oceanic carbon storage. The amount of iron-bearing dust in the atmosphere depends on climate (precipitation, wind strength, moisture) and on the extent of dust sources, which could vary due to anthropogenically or climate induced changes in vegetation cover. Increases in erosion (due to enhanced agriculture, urbanization, conversion of land for agricultural use) and the hydrological cycle will likely affect transport of iron-bearing dust to the ocean [*Tegen and Fung, 1995; Harrison et al., 2001*]. This could change the biological pump strength and alter atmosphere-ocean carbon partitioning. A similar mechanism might have worked in the past (see mechanism 1a, Section 1.1.1; *Martin, [1990]*). Note that surface nutrient availability depends on stratification and vertical mixing, which might change with climate warming as well [*Sarmiento et al., 1998*].

- b. Changes in total oceanic inventories of nutrients could be triggered by changes in the delivery of critical nutrients (N, P, Fe, Si) from external sources (rivers, atmosphere, sediments) or by changes in nitrogen fixation and denitrification rates. These processes might have occurred on glacial-interglacial time scales and could occur in the future as indirect effects of climate change [Falkowski, 1998]. If Falkowski's hypothesized link between nitrogen fixation and external iron supply exists [Falkowski, 1997], the fixed nitrogen inventory depends on the changing hydrological cycle, as it affects the availability of iron to the ocean. Changes in stratification and mixing with climate warming might also affect nitrogen fixation rates and therefore the total nitrogen inventory.
- c. Changes in the average elemental composition of organic material. Climate-related factors such as temperature, cloudiness (light availability), sea-ice extent, stratification and mixing might affect the structure of marine ecosystems. A significant shift in ecosystem structure and particularly in the composition of phytoplankton species could change the average strength of the biological pump and result in a modified $p\text{CO}_2^{\text{atm}}$ [IPCC report, 2001].

Note that mechanisms (a to c) above are analogous to mechanisms (1 to 3) proposed in Section 1.1.1 as explanations for glacial-interglacial CO_2 changes. The simple intuition gained from our three box model analysis and Eqs. 14 and 16 can help us understand how the biological pump responds to climate change.

Modeling studies of future climate have so far investigated only some of the feedback mechanisms described above. Recent studies that looked at the feedback between climate change and ocean uptake include Maier-Reimer *et al.* [1996], Sarmiento and Le Quere [1996], Sarmiento *et al.* [1998], Matear and Hirst [1999], Joos *et al.* [1999], Cox *et al.* [2000]. All of these studies performed and inter-compared two types of runs: climate control runs and global warming runs. A constant climate control run fixes CO_2 and other greenhouse gases at their pre-industrial values. Global warming simulations are based on prescribed increases of CO_2 and other greenhouse gases into the future (so-called "emission scenarios").

Sarmiento and Le Quere [1996] and Sarmiento *et al.* [1998] coupled their ocean-carbon model to the Princeton/GFDL atmosphere-ocean climate model. Their diagnostic marine biological model includes biological pump parametrizations and the full carbon system equations, and is coupled with fixed biological export fluxes. The Joos *et al.* [1999] model is highly idealized in that it uses a zonally averaged ocean model coupled to an atmospheric energy balance model, and a simplified marine biological model. The model accounts for the potential fertilization of land by elevated CO_2 . Matear and Hirst [1999]

performed simulations in a coupled atmosphere-ocean climate model similar to *Sarmiento et al.* [1998]. However, this study uses the Gent-McWilliams eddy mixing parametrization in the ocean and a prognostic parameterization of export production. These two factors have the potential to significantly alter the feedbacks between climate change and oceanic CO₂ uptake. Results from these three studies are summarized in Table 3 and are described below.

Table 3. The response of oceanic CO₂ uptake to climate-induced feedbacks in three studies discussed in the text. Climate baseline refers to simulations with anthropogenic CO₂ emissions but preindustrial ocean temperature and circulation. Percent changes refer to uptake changes for the climate simulation -based on the IPCC IS92a scenario- relative to the climate baseline. Warming and circulation effects are changes due to warming and variation in transport processes in the absence of the biological pump. “Total effect” is the uptake change when all climate feedbacks are present; “total uptake” is the cumulative ocean uptake for a model which includes all feedbacks. Note that decreases in ocean carbon uptake (i.e., negative numbers in the table) correspond to positive feedbacks relative to $p\text{CO}_2_{atm}$. *Sarmiento et al.* fix biological export fluxes while the other two studies use variable export fluxes. *Joos et al.* use a simplified, 2D ocean model coupled to an atmospheric energy balance model; the other two studies use 3D coupled atmosphere-ocean GCMs. Warming and circulation tend to decrease the oceanic uptake of CO₂, with circulation having a larger effect later on in the century, while biology increases the uptake of CO₂.

Response of Oceanic Uptake to climate-induced ocean feedbacks			
	<i>Sarmiento et al.</i> ['98]	<i>Matear and Hirst</i> ['99]	<i>Joos et al.</i> ['99]
Time Span	1990-2065	1850-2100	1765-2100
Climate Baseline (PgC)	289	402	530
Warming Effect	-11.4%	-11.9%	-12.8%
Circulation Effect	-21.8%	-10.2%	-2.8%
Biological Effect	+23.9%	+8.2%	+6.2%
Total Effect	-9.3%	-13.9%	-9.4%
Total Uptake (PgC)	262	346	480

In the context of modelling studies, the **Solubility feedback** is defined as the interaction between climate change and the ocean carbon uptake in a solubility only climate change scenario. In the absence of biology, a varying climate affects oceanic CO₂ uptake through (a) temperature or heat flux changes (SST feedback) and (b) changes in stratification and convection (circulation feedback). Note that these are precisely mechanisms 2 and 3 from the beginning of this section. The temperature and circulation effects on CO₂ uptake can be separated from each other by assuming that they are linearly independent, i.e. by neglecting nonlinearities of the carbonate chemistry. The climate simulations are therefore run in two separate abiotic models in which either the circulation or the sea surface temperature are kept constant.

Under global warming conditions, increasing SSTs cause a reduction in solubility, which drives CO_2 out of the ocean and decreases the net capacity of the ocean for taking up CO_2 . Models also predict an increase in upper water column stratification and a decrease in high latitude convective overturning with climate warming (Fig 13 e and d, respectively). Overall decreases in convection and THC result in less communication between deep and surface waters. This results in a weaker solubility pump in high latitudes, i.e., less loss of heat to the atmosphere and less CO_2 flux into the high latitude ocean.

Climate warming simulations performed with abiotic models confirm that the SST feedback and the circulation feedback are both positive feedbacks on $p\text{CO}_{2\text{atm}}$ which contribute to a decrease in the net uptake of excess CO_2 by the ocean (Table 3). In the *Sarmiento et al.* [1998] abiotic simulations, the SST feedback accounts for 82% of the decrease in cumulative uptake in CO_2 early in the simulation (years 1765-1990), while transport processes take over later on in the simulations. From 1990 to 2065, the slow-down of ocean circulation processes accounts for about 66% of the decreases in cumulative ocean uptake, with temperature increase accounting for the remaining 34%. The inclusion of the Gent-McWilliams eddy-advection scheme is hypothesized to reduce the importance of convection in the Southern Ocean and seems to account for the smaller effect of the circulation feedback of 10.2% in the *Matear and Hirst* study (Table 3). The small circulation feedback of *Joos et al.* is difficult to evaluate, since this study uses a highly simplified, two dimensional ocean model.

Biological feedback is the interaction between climate change and the uptake of CO_2 due to biological mechanisms, as described by mechanisms 4 a-c in this chapter.

The biological models used in the global climate change studies presented above are highly simplified; most of them only allow for simple changes in surface nutrient availability with climate change (mechanism 4a). The resulting biological feedbacks are necessarily tentative parameterizations of the real processes occurring in nature. In the context of our models the biological feedback is dictated only by changes in vertical stratification and the thermohaline circulation. These modify the amount of *DIC* and nutrients brought from depth by the overturning circulation, altering the strength of the natural biological pump and the CO_2 partitioning between ocean and atmosphere. Note that current thinking holds that at current CO_2 levels, increasing CO_2 in the ocean by anthropogenic addition does not directly affect biological processes in the ocean; modeling studies so far have been based on this premise.

Sarmiento et al. [1998] use a constant-biota model which fixes the export and production at their initial values. The exception are areas where phosphate becomes depleted at the surface; here, production is set to zero. In this simple model, increased stratification and slower circulation (Fig. 13e and d) lower the

upward supply of deep carbon and nutrients to the euphotic zone. The Southern Ocean is a region where deep mixing ensures communication between surface and deep waters by outcropping isopycnals. A flattening of isopycnals and a decrease in vertical mixing with climate warming reduces the communication between deep waters (rich in DIC and PO_4) and surface waters (poor in DIC and PO_4) and, in a model where biological uptake is fixed at its pre-industrial value, results in a decrease in surface-water PO_4 (Fig 13f) and accumulation of excess DIC in the deep. The biological pump becomes more effective especially in the Southern Ocean, as reflected by the large flux of CO_2 into the region. The net change due to the biological pump is a 24% increase in oceanic uptake of CO_2 (Table 3). Figure 13b provides an interesting counterpart to Figure 8 and model studies which show that the Southern Ocean biological pump reacts more strongly to nutrient depletion experiments than any other region of the ocean (see Section 1.2).

The above mechanism is equivalent to mechanism 1b in Section 1.1.1. The net effect of increased stratification and decreased Southern Ocean convective mixing in a 3 box model is a decrease in f . When biological export fluxes Π_h are fixed, a decrease in f results in a decrease in preformed nutrients PO_{4h} , in agreement with Eq. 15. The resulting depletion of nutrients acts to increase the biological pump strength and the oceanic uptake of CO_2 as shown by Eq. 14 and Figures 4 and 8.

Note that the strength of the biological feedback depends on both the physical and the biological models being used, i.e. on the specification of f and Π_h in our model. *Joos et al.* [1999] compare their standard prognostic biological model, where export fluxes are allowed to change in response to climate, to a constant export production model. Table 3 presents results from their prognostic biological model runs. In this model increased stratification and the resulting surface nutrient depletion decreases export production. This effect works against the decrease in surface nutrient supply and tends to make the biological pump less efficient. While the overall effect in the *Joos et al.* prognostic model is still an increase in the oceanic uptake of CO_2 , this increase is smaller compared to a constant export production model such as that employed by *Sarmiento et al.* [1998].

Finally, the inclusion of the Gent-McWilliams parametrization of the eddy effects [*Gent et al.*, 1995] by *Matear and Hirst* [1999] results in a smaller increase in stratification with climate change. This then results in less nutrient depletion and therefore a smaller increase in the oceanic uptake of CO_2 compared to *Sarmiento et al.* [1998]. For each of the above model studies, the negative biological feedbacks partially cancel out the positive solubility feedbacks on the oceanic uptake. The net effect of including climate change is a decrease in the oceanic uptake of CO_2 .

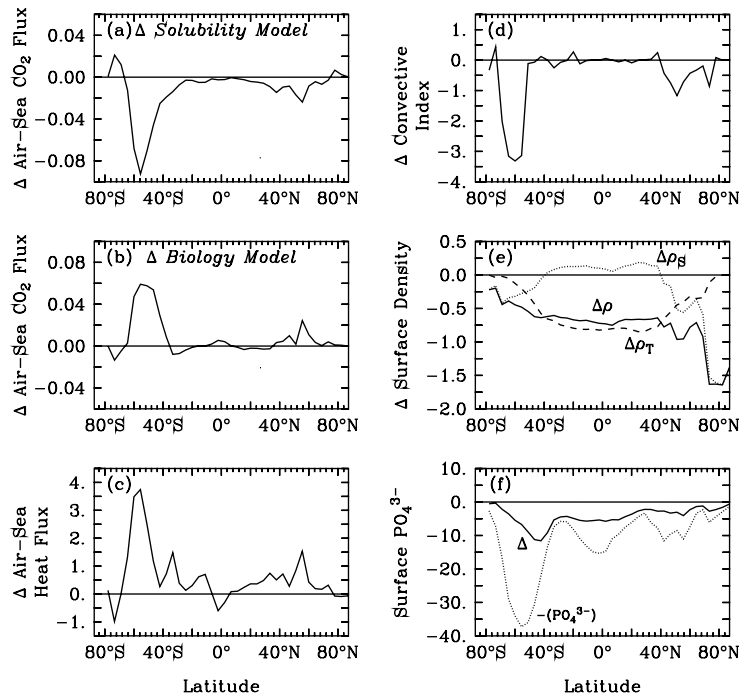


Figure 13. Figure 2 from Sarmiento *et al.* [1998] showing the Princeton GCM response to anthropogenic climate warming. Zonal integrals for the decade 2056-65 of: a. the change in air-sea CO_2 fluxes (positive for ocean uptake) due to warming and changes in ocean transport estimated by the difference between the solubility Global warming (GW) and solubility baseline (Pg/degree/yr); b. the change in air-sea CO_2 fluxes due to the biological pump calculated as the difference between the constant-biota GW and the constant biota baseline air-sea CO_2 fluxes, after removing the changes due to warming and transport (Pg/degree/yr); c. GW minus baseline heat fluxes in W/m^2 ; d. GW minus baseline of the convection index; e. Solid line: change in total surface density (GW minus control) in kg/m^3 ; dashed and dotted lines show density changes due to temperature and salinity, respectively. f. Constant biota GW minus ct. biota baseline surface PO_4^{3-} in mmol/m^2 . Dotted line is the negative of baseline PO_4^{3-} .

More recently, Bopp *et al.* [2001] investigated the response of marine productivity to climate change using two different ocean biogeochemical schemes. The first links marine export production to phosphate utilization at the surface, temperature, and light intensity but, just like the schemes above, does

not include explicit biology. The second is an NPZD (nutrient-phytoplankton-zooplankton-detritus) type model in which phytoplankton growth depends on the local conditions of light, temperature, and vertical eddy diffusion.

Interestingly, increased stratification associated with climate warming leads to both reduced nutrient supply, as in previous studies, and to increased light supply in the now thinner mixed layer. Reduced nutrient supply mainly in wintertime causes a decrease in the biological production. Increased light supply in the now more strongly stratified high latitudes gives longer growing seasons in these areas and an overall poleward shift in oceanic biological production. *Bopp et al.* find that the effect of increased light supply prevails in high latitudes, while the effect of reduced upwelling of nutrients is most important in low latitudes. As a result export production increases by 30% in high latitudes and decreases by 20% in low latitudes for a doubling of atmospheric CO₂. The overall effect is a modest decrease in export production of 6%, similar to the decrease in export production found by *Joos et al.* [1999]. One would expect that the high latitude increase in biological production will dominate, resulting in a net increase in oceanic CO₂ uptake.

The response of biology to climate change and its feedback on the system is highly dependent on the model being used (Table 3). The *Bopp et al.* study makes the point that production and surface nutrient concentration depend on a variety of mechanisms such as light availability and trophic interactions, which need to be included in future climate feedback studies. A natural next step in model development would then be to replace the nutrient based biological models with more complex, ecosystem dynamics (NPZD) type models as in the studies of *Cox et al.* [2000] and *Friedlingstein et al.* [2001].

4. SUMMARY

This chapter focuses on understanding the mechanisms responsible for the oceanic uptake of carbon. The oceanic uptake of natural CO₂ is determined by the carbon pump, which is the sum of the biological and solubility carbon pumps (Section 1). The *DIC* gradient between the surface and the deep ocean proves to be a good metric for the strength of the carbon pumps. Simple box models can help us understand the basic mechanisms underlying the variation of atmospheric *p*CO₂ between glacials and interglacials and the relationship between the biological pump strength and preformed nutrients, oceanic circulation, and gas exchange (Section 1.1).

One of the most important problems of carbon cycle research is to determine where all the anthropogenic carbon added to the oceans is going. While Section 1 analyzes the steady state oceanic uptake, Section 2 studies the transient problem, i.e., the behavior of the oceanic uptake and the corresponding atmospheric response to anthropogenic CO₂ perturbations. The uptake of ex-

cess carbon can be characterized as a sum of decaying exponential functions with time scales τ_j characteristic for different oceanic processes and with coefficients related to the relative capacities of the reservoirs j filled up with CO_2 at rates τ_j . Mixing between surface and deep waters determines the rate at which these reservoirs are being filled up. Differences in convective mixing or isopycnal mixing are thus partly responsible for differences in carbon uptake between different models.

Model studies suggest that the Southern Ocean plays a critical role in the uptake of anthropogenic CO_2 from the atmosphere (Figures 11 and 12) and in the feedback processes between the oceanic carbon cycle and climate change (Figure 13). Changes in oceanic SST, circulation, mixing, gas exchange following climate warming will result in changes of the natural biological and solubility pumps in the ocean, which will influence in their turn the further uptake of carbon by the ocean. In particular, GCM studies suggest that climate warming results in increased stratification, a decrease in the vertical component of isopycnal mixing and a decrease in convective overturning primarily in the Southern Ocean.

The resulting decrease in preformed nutrients suggests a strengthening of the biological pump and therefore an increase in the biological uptake of CO_2 . At the same time, decreasing high latitude convection results in reduced uptake by the solubility pump in the high latitude ocean. Finally, increasing SSTs cause an additional reduction in the solubility pump, driving CO_2 out of the ocean. The solubility effects win over the biological effects. According to the most recent models available, in the net, climate warming decreases the capacity of the ocean for further carbon uptake and thus represents a positive feedback on the atmospheric carbon dioxide. This result, as well as the large uncertainty associated with it, should raise a red flag and stimulate scientists to improve both models and theory in order to better understand natural and anthropogenic CO_2 uptake by the ocean.

ACKNOWLEDGMENTS

The authors are grateful for support from DOE grant DE-FG02-00ER63009.

REFERENCES

- Anderson, L.A. and J.L.Sarmiento, Redfield ratios of remineralization determined by nutrient data analysis, *Global Biogeochem. Cycles*, 8, 65-80, 1994.
- Archer, D.E., H. Kheshti, and E. Maier-Reimer, Dynamics of fossil fuel CO_2 neutralization by marine CaCO_3 , *Global Biogeochem. Cycles*, 12, 259-276, 1998.
- Archer, D.E., G. Eshel, A. Winguth, W. Broecker, R. Pierrehumbert, M. Tobis, and R. Jacob, Atmospheric $p\text{CO}_2$ sensitivity to the biological pump in the ocean, *Global Biogeochem. Cycles*, 14, 1219-1230, 2000.

- Bacastow, R.B., The effect of temperature change of the warm surface waters of the oceans on atmospheric CO₂, *Global Biogeochem. Cycles*, 10, 319-333, 1996.
- Battle, M., M. Bender, T. Sowers, P.P. Tans, J.H. Butler, J.W. Elkins, J.T. Ellis, T. Conway, N. Zhang, P. Lang, and A.D. Clarke, Atmospheric gas concentrations over the past century measured in air from firn at the South Pole, *Nature*, 383, 231-235.
- Bender, M.L., P.P. Tans, J.T. Ellis, J. Orchardo, and K. Habfast, High precision isotope ratio mass spectroscopy method for measuring the O₂/N₂ ratio of air, *Geochim. Cosmochim. Acta* 58, 4751-4758, 1994.
- Bender, M.L. and M.O. Battle, Carbon cycle studies based on the distribution of O₂ in air, *Tellus* 51B, 165-169, 1999.
- Bopp, L., P. Monfray, O. Aumont, J.-L. Dufresne, H. LeTreut, G. Madec, L. Terray, and J. Orr, Potential impact of climate change on marine export production, *Global Biogeochem. Cycles*, 15(1), 81-100, 2001.
- Brewer, P.G., Direct observation of the oceanic CO₂ increase, *Geophys. Res. Lett.*, 5(12), 997-1000, 1978.
- Broecker, W.S., Glacial to Interglacial Changes in Ocean Chemistry, *Progress in Oceanography*, 2, 151-197, 1982.
- Broecker, W.S., Ocean Chemistry during glacial time, *Geochimica et Cosmochimica Acta* 46, 1689-1705, 1982.
- Broecker, W.S., S. Sutherland, W. Smethie, TH. Peng, G. Ostlund, Oceanic radiocarbon: separation of the natural and bomb component, *Global Biogeochem. Cycles* 9(2), 263-288, 1995.
- Caldeira, K. and P.B. Duffy, The role of the Southern Ocean in Uptake and storage of anthropogenic carbon dioxide, *Science*, 287, 620-622, 2000.
- Chen, C.T.A., and F.J. Millero, Gradual increase of oceanic CO₂, *Nature*, 277, 205-206, 1979.
- Coatanoan, C., C. Goyet, N. Gruber, C.L. Sabine, and M. Warner, Comparison of two approaches to quantify anthropogenic CO₂ in the ocean: Results from the northern Indian Ocean, *Global Biogeochem. Cycles*, 15(1), 11-25, 2001.
- Cox, P.M., R.A. Betts, C.D. Jones, S.A. Spall, I.J. Totterdell, Acceleration of global warming due to carbon-cycle feedbacks in a coupled climate model, *Nature*, 408, p.184, 2000.
- Cramer, W., A. Bondeau, F.I. Woodward, I.C. Prentice, R.A. Betts, V. Brovkin, P.M. Cox, V. Fisher, J.A. Foley, A.D. Friend, C. Kucharik, M.R. Lomas, N. Ramankutty, S. Sitch, B. Smith, A. White, and C. Young-Molling, Global response of terrestrial ecosystem structure and function to CO₂ and climate change: results from six dynamic global vegetation models, *Global Change Biology*, 2001.
- DeFries R.S., R.A. Houghton, M.C. Hansen, C.B. Field, D. Skole, J. Townshend, Carbon emissions from tropical deforestation and regrowth based on satellite observations for the 1980s and 1990s, *Proceedings of the National Academy of Sciences of the United States of America* 99(22), 14256-14261, 2002.
- Dixon, K.W., T.L. Delworth, M.J. Spelman and R.J. Stouffer, The influence of transient surface fluxes on North Atlantic overturning in a coupled GCM climate change experiment, *Geophys. Res. Lett.*, 26, 2749-2752, 1999.
- Dutay, J.-C., Influence du melange vertical et de la couche melangee sur la ventilation de l'océan. Simulations numeriques des traceurs transitoires tritium-helium-3 et CFCs avec le modele OPA. Ph.D. Thesis, Univ. Pierre et Marie Curie.
- Dutay, J.-C. et al., Evaluation of ocean model ventilation with CFC-11: comparison of 13 global ocean models, *Ocean Modeling*, 4, 89-120, 2002.
- England, M.H., Using chlorofluorocarbons to assess ocean climate models, *Geophys. Res. Lett.* 22, 3051-3054, 1995.

- England, M.H., Hirst, A.C., Chlorofluorocarbon uptake in a world ocean model. Sensitivity to surface thermohaline forcing and subsurface mixing parametrizations, *J. Geophys. Res.* 102, 15709-15731, 1997.
- Falkowski, P.G., R.T. Barber, and V. Smetacek, Biogeochemical controls and feedbacks on ocean primary production, *Science*, 281, 200-206, 1998.
- Falkowski, P.G., Evolution of the nitrogen cycle and its influence on the biological sequestration of CO₂ in the ocean, *Nature*, 387(6630), 272-275, 1997.
- Feely, R.A., C.L. Sabine, R.M. Key, and T.H. Peng, CO₂ synthesis results: estimating the anthropogenic carbon dioxide sink in the Pacific ocean, US. JGOFS News, 9, 1-5, 1999.
- Friedlingstein, P., L. Bopp, P. Ciais, J.-L. Dufresne, L. Fairhead, H. LeTreut, P. Monfray, and J. Orr, Positive feedback between future climate change and the carbon cycle. Note du Pole de Modelisation, *Geophysical Research Letters*, 28, 1543-1546, 2001.
- Ganeshram, R.S., T.F. Pedersen, S.E. Calvert, and R. Francois, Reduced nitrogen fixation in the glacial ocean inferred from changes in marine nitrogen and phosphorus inventories, *Nature*, 415, 156-159, 2002.
- Gent, P.R., J. Willebrand, T.J. Mc Dougall and J.C. McWilliams, Parametrizing eddy-induced transports in ocean circulation models, *J. Phys. Oceanogr.*, 25, 463-474, 1995.
- Gildor, H., E. Tziperman and R.J. Toggweiler, The sea-ice switch mechanism and glacial-interglacial CO₂ variations, *Global Biogeochemical Cycles*, 16, 10.1029/2001GB001446, 2002.
- Gloor, M., N. Gruber, J.L. Sarmiento, C.L. Sabine, R.A. Feely, C. R  denbeck, A first estimate of present and preindustrial air-sea CO₂ flux patterns based on ocean interior carbon measurements and models, *Geophys. Res. Lett.* Vol. 30 No. 1, 2003.
- Gnanadesikan, A., R.D. Slater, N. Gruber, and J.L. Sarmiento, Oceanic vertical exchange and new production: a comparison between models and observations, *Deep Sea Res. Part II*, 49, 363-401, 2002.
- Goodale C.L., M.J. Apps, R.A. Birdsey, C.B. Field, L.S. Heath, R.A. Houghton, J.C. Jenkins, G.H. Kohlmaier, W. Kurz, S.R. Liu, G.J. Nabuurs, S. Nilsson, A.Z. Shvidenko, Forest carbon sinks in the Northern Hemisphere, *Ecological Applications*, 12(3), 891-899, 2002.
- Gruber, N. and J.L. Sarmiento, Biogeochem./Physical Interactions in Elemental Cycles, in *THE SEA: Biological-Physical Interactions in the Oceans*, edited by A. R. Robinson, J. J. McCarthy, and B. J. Rothschild, John Wiley and Sons, Volume 12, 337-399, 2002.
- Gruber, N., J.L. Sarmiento, and T.F. Stocker: An improved method for detecting anthropogenic CO₂ in the oceans. *Global Biogeochem. Cycles*, 10(4), 809-837, 1996.
- Gruber, N., Anthropogenic CO₂ in the Atlantic Ocean, *Global Biogeochem. Cycles*, 12, 165-191, 1998.
- Harrison S.P., K.E. Kohfeld, C. Roelandt, T. Claquin, The role of dust in climate changes today, at the last glacial maximum and in the future, *Earth-Science review*, 54(1-3), 43-80 Sp.Iss SI, 2001.
- Heimann, M. and Maier-Reimer, E., On the relations between the oceanic uptake of CO₂ and its carbon isotopes, *Global Biogeochem. Cycles*, 10, 89-110, 1996
- Houghton, J.T. et al., eds., Climate Change 2001: The Scientific Basis, Cambridge U. Press, New York, 2001. See <http://www.ipcc.ch>.
- Joos, F., G.K. Plattner, T.F. Stocker, O. Marchal, A. Schmittner, Global Warming and Marine Carbon Cycle Feedbacks on Future Atmospheric CO₂, *Science*, 284, 464-467, 1999.
- Joos, F., J.C. Orr, and U. Siegenthaler, Ocean carbon transport in a box-diffusion versus a general circulation model, *J. Geophys. Res.*, 102 (C6), 12367-12388, 1997.
- Keeling, R.F. and S.R. Shertz, Seasonal and interannual variations in atmospheric oxygen and implications for the global carbon-cycle, *Nature*, 358(6389), 723-727, 1992.

- Keeling, R.F., S.C. Piper, and M. Heimann, Global and hemispheric CO_2 sinks deduced from changes in atmospheric O_2 concentrations, *Nature*, 381, 218-221, 1996.
- Keeling, R.F. and H.E. Garcia, The change in oceanic O_2 inventory associated with recent global warming, *Proceedings of the National Academy of Sciences of the United States of America*, 99(12), 7848-7853, 2002.
- Knorr, W., and M. Heimann, Uncertainties in global terrestrial biosphere modeling, Part I: a comprehensive sensitivity analysis with a new photosynthesis and energy balance scheme, *Global Biogeochem. Cycles*, 15(1), 227-246, 2001.
- Knox, F., and M.B. McElroy, Changes in atmospheric CO_2 : Influence of the marine biota at high latitude, *J. Geophys. Res.*, 89, 4629-4637, 1984.
- Knutti, R. and T.F. Stocker, Influence of the thermohaline circulation on projected sea level rise, *J. Clim.*, 13, 1997-2001, 2000.
- Maier-Reimer, E., U. Mikolajewicz, and A. Winguth, Future ocean uptake of CO_2 - Interaction between ocean circulation and biology, *Climate Dynamics*, 12, 711-721, 1996.
- Maier-Reimer, E. and K. Hasselmann, Transport and storage of CO_2 in the ocean - an inorganic ocean-circulation carbon cycle model, *Climate Dynamics*, 2, 63-90, 1987.
- Manabe, S. and R.J. Stouffer, Century-scale effects of increased atmospheric CO_2 on the ocean-atmosphere system, *Nature*, 364, 215-218, 1993.
- Manning, A.C., Temporal variability of atmospheric oxygen from both continuous measurements and a flask sampling network: Tools for studying the global carbon cycle. Ph. D. thesis, U.C. San Diego, La Jolla, California, U.S.A., 190p.
- Marinov, I., A. Gnanadesikan, J.L. Sarmiento, and R.D. Slater, The biological carbon pump: influence of nutrient depletion and circulation, in preparation.
- Martin, J.H., Glacial-Interglacial CO_2 change: the iron hypothesis, *Paleoceanography*, Vol. 5, no. 1, 1-13, 1990.
- Matear, R.J. and A.C. Hirst, Climate change feedback on the future oceanic CO_2 uptake, *Tellus*, 51B(3), 722-733, 1999.
- Matear, R.J., Effects of numerical advection schemes and eddy parametrizations on ocean ventilation and oceanic anthropogenic CO_2 uptake, *Ocean Modelling*, 3: 217-248, 2001.
- McElroy, M.B., Marine biological controls on atmospheric CO_2 and climate, *Nature*, 302, 328-329, 1983.
- McNeil, B.I., B. Tilbrook, and R.J. Matear, Accumulation and uptake of anthropogenic CO_2 in the Southern Ocean, south of Australia between 1968 and 1996, *JGR-Oceans*, 106, 31431-31445, 2001.
- McNeil, B.I., R.J. Matear, R.M. Key, Bullister, J.L. Sarmiento, Anthropogenic CO_2 uptake using the global CFC data-set, *Science*, 299, 235-239, 2003.
- Mikolajewicz, U. and R. Voss, The role of the individual air-sea flux components in CO_2 -induced changes of the ocean's circulation and climate, *Clim. Dyn.*, 16, 627-642, 2000.
- Murnane, R.J., J.L. Sarmiento, C. LeQuere, Spatial distribution of air-sea fluxes and the interhemispheric transport of carbon by the oceans, *Global Biogeochem. Cycles*, v.13, no 2, 287-305, 1999.
- Najjar, R. and J. Orr, Design of OCMIP-2 simulations of chlorofluorocarbons, the solubility pump and common biogeochemistry, <http://www.ipsl.jussieu.fr/OCMIP>.
- Orr, J.C., Ocean Carbon-cycle Intercomparison Project (OCMIP). Phase I (1995-1997). IGBP/GAIM Report Series, Report no. 7.
- Orr, J.C., E. Maier-Reimer, U. Mikolajewicz, P. Monfray, J.L. Sarmiento, J.R. Toggweiler, N.K. Taylor, J. Palmer, N. Gruber, C.L. Sabine, C.L. Le Quere, R.M. Key, and J. Boutin, Estimates of anthropogenic carbon uptake from four three-dimensional global ocean models, *Global Biogeochem. Cycles*, 15(1), 43-60, 2001.

- Pacala, S.W., et al., Consistent land- and atmosphere-based US carbon sink estimates, *Science*, 292(5525), 2316-2320, 2001.
- Peng, T.H., R. Wanninkhof, J.L. Bullister, R.A. Feely, and T. Takahashi, Quantification of decadal anthropogenic CO₂ uptake in the ocean based on dissolved inorganic carbon measurements, *Nature*, 396, 560-563, 1998.
- Petit, J.R. et al, Climate and atmospheric history of the past 420,000 years from the Vostok ice core, Antarctica, *Nature*, 399, 429-436, 1999.
- Plattner, G.K., F. Joos, T.F. Stocker, O. Marchal, Feedback mechanisms and sensitivities of ocean carbon uptake under global warming, *Tellus Series-B- chemical and physical meteorology* 53(5), 564-592, 2001.
- Plattner, G.K., F. Joos, T.F. Stocker, Revision of the global carbon budget due to changing air-sea oxygen fluxes, *Global Biogeochem. Cycles*, 16(4), art. 1096, 2002.
- Robitaille, D.Y. and A.J. Weaver, Validation of sub-grid-scale mixing schemes using CFCs in a global ocean model. *Geophys. Res. Lett.* 22, 2917-2920, 1995.
- Sabine, C.L., R.M. Key, K.M. Johnson, F.J. Millero, A. Poisson, J.L. Sarmiento, D.W.R. Wallace, and C.D. Winn, Anthropogenic CO₂ inventory of the Indian Ocean, *Global Biogeochem. Cycles*, 13, 179-198, 1999.
- Sabine, C.L., Feely RA, Key RM, Bullister JL, Millero FJ, Lee K, Peng TH, Tilbrook B, Ono T, and Wong CS, Distribution of anthropogenic CO₂ in the Pacific Ocean, *Global Biogeochem. Cycles*, 16(4), 1083, 2002.
- Sarmiento, J.L. and J.R. Toggweiler, A new model for the role of the oceans in determining atmospheric pCO₂, *Nature*, 308, 620-624, 1984.
- Sarmiento, J.L., J.C. Orr, and U. Siegenthaler, A perturbation simulation of CO₂ uptake in an ocean general- circulation model, *J. Geophys. Res.-Oceans*, 97, 3621-3645, 1992.
- Sarmiento, J.L., C. Le Quere, S.W. Pacala, Limiting future atmospheric carbon-dioxide, *Global Biogeochem. Cycles*, 9(1): 121-137, 1995.
- Sarmiento, J.L. and C. Le Quere, Oceanic carbon dioxide uptake in a model of century scale global warming, *Science*, 274, 1346-1350, 1996.
- Sarmiento, J.L., T.M.C. Hughes, R.J. Stouffer, and S. Manabe, Simulated response of the ocean carbon cycle to anthropogenic climate warming, *Nature*, 393, 245-249, 1998.
- Sarmiento, J.L. and N. Gruber, Sinks for anthropogenic carbon, *Physics Today*, 55(8), 30-36, 2002.
- Schiller, A., U. Mikolajewicz and R. Voss, The stability of the North Atlantic thermohaline circulation in a coupled ocean-atmosphere general circulation model, *Clim. Dyn.*, 13, 325-347, 1997.
- Schmittner, A. and T.F. Stocker, The stability of the thermohaline circulation in global warming experiments, *J.Clim.*, 12, 1117-1133, 1999.
- Shackleton, N.J., Carbon-13 in Uvigerina: tropical rainforest history and the equatorial Pacific carbonate dissolution cycles, *The fate of fossil fuel CO₂ in the Oceans*, Plenum Press, p. 401-427, 1977.
- Shackleton, N.J., The 100,000-year ice-age cycle identified and found to lag temperature, carbon dioxide, and orbital eccentricity, *Science*, 289, 1897-1902, 2000.
- Siegenthaler, U. and H. Oeschger, Predicting future atmospheric carbon-dioxide levels, *Science*, 199, 388-395, 1978.
- Siegenthaler, U. and T.H. Wenk, Rapid atmospheric CO₂ variations and ocean circulation, *Nature*, 308, 624-626, 1984.
- Siegenthaler, U., Uptake of excess CO₂ by an outcrop-diffusion model of the ocean, *J. Geophys. Res.*, 88, 3599-3608, 1983.
- Sigman, D.M. and E.A. Boyle, Glacial/interglacial variations in atmospheric carbon dioxide, *Nature*, 407, 859-869, 2000.

- Stephens B.B. and R.F. Keeling, The influence of Antarctic sea ice on glacial-interglacial CO₂ variations, *Nature*, 404, 171-174, 2000.
- Stocker, T.F. and A. Schmittner, Influence of CO₂ emission rates on the stability of the thermohaline circulation, *Nature*, 388, 862-865, 1997.
- Stouffer, R.J. and S. Manabe, Response of a coupled ocean-atmosphere to increasing atmospheric carbon dioxide: sensitivity to the rate of increase, *J. Clim.*, 12, 2224-2237, 1999.
- Takahashi, T., R.H. Wanninkhof, R.A. Feely, R.F. Weiss, D.W. Chipman, N. Bates, J. Olafsson, C. Sabine, and S.C. Sutherland, Net sea-air CO₂ flux over the global oceans: An improved estimate based on the sea-air *pCO*₂ difference, in *Proceedings of the 2nd International Symposium, CO₂ in the Oceans, extended abstracts*, ed. by Yukihiko Nojiri, Center for Global Env Research, Tsukuba, Japan, 1999.
- Tegen, I., and I. Fung, Contribution to the atmospheric mineral aerosol load from land surface modification, *J. Geophys. Res.*, 100, 18707-18726, 1995.
- Toggweiler, J.R., Variation of atmospheric CO₂ by ventilation of the ocean's deepest water, *Paleoceanography*, 14, 571-588, 1999.
- Toggweiler, J.R., R. Murnane, S. Carson, A. Gnanadesikan, and J.L. Sarmiento, Representation of the carbon cycle in box models and GCMs - 1. Solubility pump, *Global Biogeochem. Cycles*, 17(1), 1026, doi:10.1029/2001GB001401, 2003.
- Toggweiler, J.R., R. Murnane, S. Carson, A. Gnanadesikan, and J.L. Sarmiento, Representation of the carbon cycle in box models and GCMs - 2. Organic pump, *Global Biogeochem. Cycles*, 17(1), 1027, doi:10.1029/2001GB001841, 2003.
- Volk, T. and M.I. Hoffert, Ocean carbon pumps: Analysis of relative strengths and efficiencies in ocean driven atmospheric CO₂ changes, in *The Carbon Cycle and Atmospheric CO₂: Natural variations Archaean to present*, ed. by E.T. Sundquist and W.S. Broecker, Geophys. Monogr. Ser., 32, 99-110, AGU, Washington, D.C., 1985.
- Wallace, Monitoring global ocean carbon inventories. *Ocean Observing System Development Panel, OOSDP Background Report, 5*, Texas AM University, Texas, 1995.
- Wanninkhof, R., Relationship between gas exchange and wind speed over the ocean, *J. Geophys. Res.*, 97, 7373-7382, 1992.

..